fluids

MDPI

Article

Cavitation Strength, Acoustic Nonlinearity, and Gas Bubble Distribution in Water

Alexey V. Bulanov *, Ekaterina V. Sosedko, Vladimir A. Bulanov and Igor V. Korskov

V.I. Il'ichev Pacific Oceanological Institute Far Eastern Branch of the Russian Academy of Sciences, 43 Baltiyskaya Str., 690041 Vladivostok, Russia; s_kat@mail.ru (E.V.S.); bulanov@poi.dvo.ru (V.A.B.); i_korskov@poi.dvo.ru (I.V.K.)

* Correspondence: a_bulanov@me.com; Tel.: +7-(423)-237-4913; Fax: +7-(423)-231-2573

Abstract: The acoustic properties of real liquids are largely related to the phase inclusions contained in them, of which gas bubbles are the most common. The aim of the work was to find the relationship between the nonlinear acoustic parameter and the cavitation strength of the liquid with the distribution of bubbles in the liquid, which has so far been poorly studied. The theoretical studies of the parameter of acoustic nonlinearity and the cavitation strength of a liquid with bubbles were carried out within the framework of the homogeneous approximation of a micro-homogeneous liquid; the relationship of these parameters with the bubble distribution function was established, and the typical values of these parameters for different concentrations of bubbles were calculated. Experimental measurements of the parameter of acoustic nonlinearity and the cavitation strength in the upper layer of seawater were carried out; these measurements were consistent with the theoretical estimates. A connection was established between the thresholds of acoustic and optical cavitation—the optical breakdown of a liquid by laser radiation. The results obtained can find practical application in the measurement of the cavitation strength of seawater at great depths in the sea, and the use of an optoacoustic method associated with the use of optical cavitation is proposed.

Keywords: nonlinear acoustic parameter; cavitation strength; optical breakdown; seawater; bubbles; laser radiation

Citation: Bulanov, A.V.; Sosedko, E.V.; Bulanov, V.A.; Korskov, I.V. Cavitation Strength, Acoustic Nonlinearity, and Gas Bubble Distribution in Water. *Fluids* **2024**, *9*, 3. https://doi.org/10.3390/fluids9010003

Academic Editors: D. Andrew S. Rees and Rui Han

Received: 1 November 2023
Revised: 14 December 2023
Accepted: 20 December 2023
Published: 24 December 2023

1. Introduction

The important properties of liquids include their nonlinear properties [1–4], which are characterized by a nonlinear acoustic parameter, as well as cavitation strength—a discontinuity of the continuity of a liquid at high intensities in an acoustic wave. The manifestation of nonlinear effects is greatly facilitated by the presence of various nuclei in the liquid–gas bubbles, foreign particles, and other inclusions of various origins [3–6]. For practical applications, it is important to study the properties of real liquids with inclusions in them. Bubbles occupy a special position among the inclusions of various natures contained in liquids, which, as a rule, most significantly affect the acoustic characteristics of liquids [3–5,7–13]. Such characteristics usually include linear acoustic characteristics—the speed of sound, the coefficient of absorption, and the scattering of sound [1,6].

The study of linear acoustic characteristics in liquids began to be studied at the very beginning of the history of acoustics. In the second half of the 20th century, the intensive study of the nonlinear acoustic properties of liquids was originated [1–3]. A special interest in nonlinear acoustics appeared in connection with the creation and implementation of fundamentally new nonlinear acoustic parametric emitters with the unique properties of broadband and high radiation directivity [1–4,14]. However, it turns out that the nonlinear characteristics of liquids are among the parameters that strongly affect the efficiency of such radiators. These primarily include the cavitation strength of liquids, which fundamentally limits the possible achievable power of emitters due to the appearance of a discontinuity in the continuity of the liquid near the emitting surfaces at high sound intensities [4–6,14].

Another important nonlinear characteristic of a liquid that affects the efficiency of any acoustic systems operating at high energy densities is the parameter of the acoustic nonlinearity of the liquid [1–4,14]. In addition, it turns out that this parameter can vary greatly in the presence of various micro-inhomogeneities in the liquid and especially in the presence of bubbles [3,4,7,14,15]. Therefore, along with the tasks of directly studying the nonlinear properties of liquids, the studies of bubble distributions in real liquids are becoming important [7–13].

The studies of the functions of bubble size distribution in liquid media have a long history; however, to date, there remain questions related to both the diagnosis of bubbles and the concentration of bubbles; these issues are mainly related to natural liquids—water in various reservoirs, including seawater [8–13]. Thus, the characteristics of the liquid indicated in the title of the article turn out to be mutually related by practical application, and it is of interest to study them comprehensively in relation to real liquids. At the same time, the relationship of these different nonlinear acoustic characteristics of micronuclear liquids has so far been poorly studied [1,4,5,14,15]. Therefore, the issues related to the study of the nonlinear characteristics of micro-homogeneous liquids are among the fundamental issues of modern acoustics, which are also in demand in practice.

Unfortunately, the nonlinear characteristics of liquids are difficult to study in simple ways [1–5]. These characteristics include the cavitation strength or tensile strength of a liquid [4,5,16,17]. Cavitation strength is associated with the presence of the nuclei of a new phase in the liquid. For water in marine conditions, the issue of cavitation strength has turned out to be particularly difficult. It turns out that the presence of the phase inclusions of the various natures specific to marine conditions (gas bubbles, suspensions, plankton, etc.) leads to an unusual behavior of the cavitation strength of seawater. In various regions of the world ocean, on the one hand, it turns out that it depends on geographical latitude; on the other hand, it turns out to be unusually low, even having a value less than hydrostatic pressure [5,15,16]. Therefore, one of the issues to be studied in this work is the question of the relationship of cavitation strength with the bubbles distributed in a liquid.

The nonlinear acoustic parameter ε is also very sensitive to the presence of micro-inhomogeneities in water [1–4]. Therefore, in particular, it can be used to diagnose a real liquid, including seawater. Usually, measurements of the parameters of the thermodynamic state of a liquid and the speed of sound—the first derivative $c = (\partial\rho/\partial P)_S{}^{-1/2}$ (where ρ is density, P is pressure, and S is entropy)—are used to study the ocean by acoustic methods. However, the entire history of the development of physics indicates that not only the first derivatives but also the following derivatives of the parameters of the medium can also turn out to be important characteristics that reveal the state of the medium. We believe that for these purposes, we can try to use a parameter ε associated with the second derivative of the equation of state $\Gamma = \rho\left(\partial c^2/\partial P\right)_S$, which can become an informative feature for diagnosing a real liquid, including seawater. The nonlinear acoustic parameter is related to the ratio [1–4]:

$$\varepsilon = 1 + (\rho/2)\left(\partial c^2/\partial P\right)_S \equiv 1 + \Gamma/2 \quad (1)$$

In liquids containing various phase inclusions, the nonlinearity parameter may increase significantly. For liquids containing gas bubbles, the nonlinearity parameter ε will depend on the size distribution of the bubbles, as well as on the dynamic characteristics of the bubbles at different frequencies of acoustic disturbances [3,4,7]. Despite the importance of the nonlinearity parameter for the marine environment, information on its measurements at sea is very scarce [1–4,7,15,18]. An important task to be solved in this work is the establishment of the relationship of the nonlinear parameter ε with the distribution of bubbles and the cavitation strength.

The issue of practical methods for measuring cavitation strength in marine conditions, especially at great depths, remains relevant. As a rule, acoustic methods are used, and mainly low-frequency methods (no more than a dozen kHz) are used [4,5,16]. However, due to the successful application of nonlinear parametric emitters in oceanographic re-

search, the question of the cavitation strength of seawater under the influence of relatively high-frequency pumping, which can be hundreds of kHz, up to units of MHz, remains open [3,4,14]. In this connection, the question of the behavior of the acoustic nonlinearity parameter at the corresponding frequencies also arises; this behavior is directly related to the efficiency and stability of the characteristics of the parametric radiators.

Due to the difficulties involved in measuring cavitation strength by acoustic methods, other methods are being sought. These include optoacoustic methods [17,19,20]. Under the action of laser radiation in a liquid, an optical breakdown occurs, along with the appearance of cavities filled with plasma in the liquid, a kind of optical cavitation, accompanied by a strong sound generation effect [19,20]. The spectrum of such radiation is directly related to the breakdown dynamics—the formation and dynamics of a breakdown cavity in a liquid. The interaction process is short-term, but at the same time, most of the laser radiation (up to 40–50%) is converted into acoustic radiation [20–24].

To date, the relationship between the optical breakdown thresholds and the cavitation strength of a real liquid has been poorly studied; therefore, it turns out to be relevant to study the mechanisms of optical breakdown generation in a liquid (especially in seawater) and to establish a connection with cavitation strength [22–24]. In such conditions, the question arises about the possibility of the practical application of laser radiation to study the nonlinear properties of a liquid—cavitation strength, distribution of the nuclei of a new phase, etc.

In this paper, the features of the nonlinear acoustic characteristics of seawater containing bubbles, as well as the characteristics of cavitation strength and the possibility of evaluating the cavitation strength of water by the optoacoustic method, are discussed.

2. Theoretical Foundations

2.1. Methods of the Acoustic Nonlinearity Measuring

As the main approximation, we consider a micro-inhomogeneous liquid in a homogeneous approximation, i.e., we consider the wavelength of sound λ to be much larger than the average distance l between heterogeneous inhomogeneities (bubbles, suspensions, plankton, etc.), which, in turn, is much larger than the radius of inhomogeneity R, i.e., $R << l << \lambda$. We also require that the sound scattering sections on the inhomogeneities σ (including the resonance of the bubbles) do not overlap, i.e., $l > \sqrt{\sigma}$. In addition, we consider the amplitudes of the pumping waves P_1 and P_2 with frequencies ω_1 and ω_2 that are not too large; thus, we can ignore the effects of nonlinear attenuation and use the constant pumping approximation [3,14]. Under the assumptions made, the equation describing the generation of a quasi-plane wave of difference frequency $\Omega = \omega_1 - \omega_2$ can be written as [3,7,18]:

$$\nabla^2 P_\Omega - \frac{1}{c^2}\frac{\partial^2 P_\Omega}{\partial t^2} = -\frac{\varepsilon_e}{\rho c^4}\frac{\partial^2}{\partial t^2}({P_1}^* P_2) \quad (2)$$

Here, ε_e is an effective nonlinear parameter that takes into account the nonlinearity of a pure liquid and the nonlinearity introduced by micro-inhomogeneities.

An important parameter for determining ε is the distance at which nonlinear effects develop—the rupture distance in the wave. The nonlinear acoustic parameter ε is directly related to the Riemann solution [3] in the evolution of simple waves, according to which the propagation velocity of a simple wave is $c = c_0 + \varepsilon v$, where c_0 is the adiabatic speed of sound and v is the velocity of particles in the wave. The appearance of the dependence of the wave propagation velocity on its amplitude leads to distortions of the wave profile up to the formation of shock waves. The distance at which a plane harmonic wave degenerates into a shock wave is commonly called the rupture distance r^*, which is determined by the ratio [3] $r^* = 1/\varepsilon k M$, where $k = \omega/c$ is the wave number and $M = v/c = P/\rho c^2$ is the Mach number. By measuring the distance r^* at which nonlinear harmonics appear in the wave, it is possible to determine the nonlinear acoustic parameter ε by the formula [25]:

$$\varepsilon = \rho c^3/(\omega P_\omega r^*). \quad (3)$$

In practice, a relative method of measuring a nonlinear acoustic parameter is often used, which consists of the preliminary calibration of the meter in a known medium and then the calculations of ε according to the formula $\varepsilon = \varepsilon_0 \cdot (U_\Omega / U_{\Omega 0})$, where ε_0 and $U_{\Omega 0}$ are the values corresponding to the reference sample [2,3] and U_Ω is the amplitude of the signal in real measurements.

A more universal method, which allows the measurement of the frequency features of the acoustic nonlinearity parameter, is to measure the amplitude of the waves of the difference frequency P_Ω and pumping P_ω at a different distance r. The basis of the method is based on the solution in [3], which can be written as:

$$\frac{v_{2\omega}}{v_\omega} = \frac{1}{2\alpha_\omega r^*}(e^{-2\alpha_\omega r} - e^{-4\alpha_\omega r}) \tag{4}$$

where $r^* = 1/\varepsilon kM$ is the rupture distance and α_ω is the sound absorption coefficient at the frequency ω. It can be seen from Formula (4) that the amplitude of the second harmonic increases to a distance $r_m = \ln 2/(2\alpha_\omega)$, where it has a maximum equal to $v_{2\omega}/v_\omega = 1/(8\alpha_\omega r^*)$, and then abruptly decays, obeying the exponential law. The latter solution is valid when $\alpha_\omega r_* > 1$, i.e., when the attenuation length is less than the rupture length. Very often, the opposite case occurs when $\alpha_\omega r_* < 1$. Then, the solution is valid only at small distances $r < r_m$, when nonlinear effects do not have time to develop. In this case, using $\alpha_\omega r << 1$, the following simple expression $v_{2\omega}/v_\omega = r/r^*$ is obtained. We consider the behavior of the wave only on a linear section $r < r^*$, while it is more convenient to switch to pressure $P = \rho c v$; then, we obtain:

$$P_{2\omega} = \left(\varepsilon_{2\omega}\omega/\rho c^3\right) P_\omega r. \tag{5}$$

In the more complex and the most practically important case of using a biharmonic signal with the frequencies ω_1 and ω_2, it can be shown that in a linear section $r < r^*$, the generation of a signal with a difference frequency $\Omega = \omega_1 - \omega_2$ is described by the formula:

$$P_\Omega = \left(\varepsilon_\Omega/\rho c^3\right)_e \Omega {P_\omega}^2 r \tag{6}$$

Parametric emitters (PE), combining broadband with the maintenance of high directivity in a large frequency range, have recently acquired an important role in hydroacoustics [3,14]. The calculation of the amplitude of the difference frequency wave can be obtained using Equation (2), which includes the acoustic nonlinearity parameter in the right part. Thus, the efficiency of PE is related to the magnitude; therefore, PE can be used to determine the magnitude of a nonlinear acoustic parameter [3,18,25].

As a result of solving Equation (2) under the assumptions made above, it is possible to obtain several limiting expressions for the difference frequency wave field, from which it is possible to obtain the corresponding expressions and to allow, in practice, the calculation of the nonlinear parameter by the following formulas:

(a) Valid for the far field in the Berktay mode of a parametric emitter [3,14]:

$$\varepsilon = 4P_\Omega(r) r e^{\alpha_\Omega r} / [D_\Omega R_F P_0 \ln[2\alpha_\omega R_F \gamma_E / (\Omega/\omega)]], \tag{7}$$

where $R_F = k_\omega d^2/8$ is the Fraunhofer parameter; $D_\Omega = k_\Omega d/4$; $\gamma_E = 1.78$ is the Euler constant; $P_0 = P_{\omega 1} P_{\omega 2}/\rho c^2$; and α_ω and α_Ω are the damping coefficients of the pump wave and the difference frequency wave, respectively.

(b) In conditions when the nonlinear interaction zone is determined not by the spherical divergence of the beams, but by attenuation at the pumping frequency, which corresponds to the Westervelt regime, the nonlinear parameter ε is determined by the formula:

$$\varepsilon = 2\alpha_\omega r P_\Omega(r) e^{\alpha_\Omega r} / \left[{D_\Omega}^2 P_0 [1 - \exp(2\alpha_\omega r)]\right], \tag{8}$$

which, along with the above values, also includes the sound absorption coefficient at the pump frequency α_ω, which was previously measured in each experiment.

The most practical method is considered to be the Berktay mode. In this mode, most of the PE used in practice operate in the pumping frequency range of 100–300 kHz. Here, it is necessary to take into account the divergence of the biharmonic pumping beam in the far field with relatively weak absorption at a high frequency. In this case, the nonlinear parameter can be determined by the following formula [25]:

$$\varepsilon = A(\omega,\Omega)\frac{P_\Omega r}{P_{\omega 1}P_{\omega 2}},\ A(\omega,\Omega) = \frac{4\rho c^3}{R_{F\omega}^2\Omega\ln(2\gamma_E N_A^{-2})}. \tag{9}$$

where $P_{\omega 1}$, $P_{\omega 2}$, P_Ω are the pressure amplitudes of the pumping waves with frequencies ω_1 and ω_2, and the difference frequency Ω ($\omega_{1,2} = 2\pi f_{1,2}$, $\Omega = 2\pi F$, $F = f_1 - f_2$); $N_A = (\alpha_\omega R_{F\omega})^{1/2}$; γ_E=1.78 is the Euler constant; $R_{F\omega} = k_\omega d^2/8$ is the length of the near zone at the frequency ω; $k_\omega = \omega/c$; and d is the aperture of the emitter.

2.2. Effective Parameters of a Micro-Inhomogeneous Liquid

The basic assumptions of the homogeneous continuum model, formulated in Section 2.1, make it possible to write the effective parameters of a micro-homogeneous fluid without detailed knowledge of its structure. Thus, the effective density ρ_e is obtained directly from the condition of preserving the mass of a unit volume of a micro-homogeneous liquid in the form of [3]:

$$\rho_e = \rho(1-x) + \rho' x,\quad x = \frac{4}{3}\pi\int_{R_{\min}}^{R_{\max}} R^3 g(R)dR, \tag{10}$$

where ρ and ρ' are, respectively, the density of liquid and gas in phase inclusions (bubbles, suspensions, etc.); the strokes hereafter refer to the phase inclusions; x is the volume concentration of the inclusions. Here, $g(R)$ is the size distribution function of the phase inclusions; it is defined in terms of the amount of phase inclusions per radius interval dR and is related to the concentration N (the total amount of inclusions per unit volume of liquid) by the formula $N = \int_0^\infty g(R)dR$ [3]. The dimension $g(R)$ is then defined as cm^{-4} or m^{-4}; however, usually in practice, the number of bubbles in the volume of m^3 falling within the radius range of 1 μm is taken to determine $g(R)$, so that $[g(R)] \to \mathrm{m}^{-3}\mathrm{mkm}^{-1}$ [3,4,18]. The effective compressibility of a micro-inhomogeneous liquid β_e, taking into account the resonant and relaxation characteristics of the inclusions, is [18]:

$$\beta_e = \frac{\beta}{\gamma}\left\{1 - x + \hat{X}\frac{\beta'/\gamma'}{\beta/\gamma}\left[1 - \left(1 - \frac{\rho'}{\rho}\right)\left(1 - \frac{\mathcal{K}(R,\omega)}{\beta'/\gamma'}\right)\right]\right\}. \tag{11}$$

Here, the value $\hat{X}f$ means an integral expression $\hat{X}f = \frac{4}{3}\pi\int_{R_{\min}}^{R_{\max}} dRg(R)R^3 f(R)$, from which, in the case of constancy f, we have $\hat{X}f = xf$. The value of $\gamma = C_P/C_V$ is the adiabatic constant; C_P and C_V are the heat capacity at constant pressure and volume, respectively; $\beta = (1/\rho)(\partial\rho/\partial P)_T$ is the coefficient of isothermal compressibility, which differs from the coefficient of adiabatic compressibility $\beta/\gamma = (1/\rho)(\partial\rho/\partial P)_S = \beta - \alpha^2 T/\rho C_p$ by an amount γ, where T, P, and S are the temperature, pressure, and entropy; and $\alpha = (1/\rho)(\partial\rho/\partial T)_P$ is the coefficient of thermal expansion at constant pressure. The compressibility of the inclusion $(1/V_R)\partial V_R/\partial R = (3/R)\partial R/\partial P \equiv \mathcal{K}$ differs from the adiabatic and isothermal compressibility and takes into account the resonant properties of the inclusion (for example, the resonant frequency of bubbles ω_0) and thermal relaxation, depending on the frequency of the sound and the size of the inclusion in the form of [18]:

$$\mathcal{K} = \frac{K(R,\omega)}{q(R,\omega)}, \tag{12}$$

$$K(R,\omega) = \frac{\beta'}{\gamma'} + \alpha' d'_S \varphi(k'_T R),\ q(R,\omega) = 1 - \frac{\omega^2}{{\omega_0}^2} - i\delta(R,\omega), \tag{13}$$

$${\omega_0}^2 = \frac{3}{\mathrm{Re}(K)\rho R^2}\left[1 - \frac{\mathrm{Re}(K)}{3}\frac{2\sigma}{R}\right], \tag{14}$$

$$\delta(R,\omega) = \delta_T(R,\omega) + \delta_r(R,\omega) + \delta_\eta(R,\omega) = \frac{\mathrm{Im}(K)}{\mathrm{Re}(K)} + \frac{\omega^2}{{\omega_0}^2}\left[\frac{\omega R}{c} + \frac{4\nu}{\omega R^2}\right], \tag{15}$$

$$\varphi({k'}_T R) = 3\frac{({k'}_T R)cth({k'}_T R) - 1}{({k'}_T R)^2}, \tag{16}$$

where ${k'}_T = \sqrt{i\omega/\chi'}$ is the wave number of the heat wave; χ' is the coefficient of thermal conductivity of the gas; $d'_S = (dT'/dP')_{S'} = \alpha' T'/\rho' C'_{P'}$ is the slope of the adiabatic curve; ν is the coefficient of kinematic viscosity of the liquid; and σ is the coefficient of surface tension for the inclusion. The compressibility of the inclusion $\mathcal{K} = \mathcal{K}(R,\omega)$ in the limit of the small sizes tends to isothermal compressibility β'; at large sizes, it tends to adiabatic compressibility ${\beta'}_S = \beta'/\gamma'$, while at resonance $\omega = \omega_0$ the absolute value of compressibility increases sharply, by a factor of approximately $1/|\delta(R,\omega_0)|$.

A generalization of Wood's formula for the effective speed of sound $\widetilde{c}_e$ in a micro-inhomogeneous liquid is written in the form [3,14,18] $\widetilde{c}_e = [\rho_e \beta_e]^{-1/2}$, where the real part $c_e = \mathrm{Re}(\widetilde{c}_e)$ and the imaginary part $\alpha = \omega \mathrm{Im}(1/\widetilde{c}_e)$ determine the phase velocity c_e and the absorption coefficient α of the pressure wave in the form:

$$c_e = c\mathrm{Re}\left[\left\{1 - x + \frac{{\beta'}_S}{\beta_S}\hat{X}\left[1 - \left(1 - \frac{\rho'}{\rho}\right)\left(1 - \frac{\mathcal{K}(R,\omega)}{{\beta'}_S}\right)\right]\right\}\left(1 + \frac{\rho' - \rho}{\rho}x\right)\right]^{-1/2}, \tag{17}$$

$$\alpha = \frac{\omega}{c}\mathrm{Im}\left[\left\{1 - x + \frac{{\beta'}_S}{\beta_S}\hat{X}\left[1 - \left(1 - \frac{\rho'}{\rho}\right)\left(1 - \frac{\mathcal{K}(R,\omega)}{{\beta'}_S}\right)\right]\right\}\left(1 + \frac{\rho' - \rho}{\rho}x\right)\right]^{1/2} + \alpha_0, \tag{18}$$

where α_0 is the absorption coefficient of sound in pure liquid without any inclusions. In particular, for a liquid with bubbles, for which $\rho' << \rho$ and $\beta << \beta'$, Formulas (17) and (18) are simplified:

$$c_e = c\mathrm{Re}\left[\left\{1 + \hat{X}\frac{\mathcal{K}(R,\omega)}{\beta_S}\right\}(1 - x)\right]^{-1/2} \tag{19}$$

$$\alpha = \frac{\omega}{c}\mathrm{Im}\left[\left\{1 + \hat{X}\frac{\mathcal{K}(R,\omega)}{\beta_S}\right\}\right]^{1/2} + \alpha_0 \tag{20}$$

Depending on the volume concentration of bubbles x, simpler formulas can be obtained:

$$c_e \approx \begin{cases} c\left(1 - xc^2/2{c'}^2\right), & x << x_* \sim 0.05 \\ c'/\sqrt{x}, & 1 > x > x_* = {c'}^2/{c^2}_T \end{cases}, \tag{21}$$

$$\alpha \approx \begin{cases} \omega(\rho c/2)\mathrm{Im}\left[\hat{X}\mathcal{K}(R,\omega)\right], & x << x_* \\ \omega\sqrt{\rho}\mathrm{Im}\sqrt{\hat{X}\mathcal{K}(R,\omega)}, & 1 > x > x_* \end{cases} + \alpha_0. \tag{22}$$

Taking into account Formula (1) for the nonlinear parameter ε and using Formulas (12)–(16), it is possible to calculate the effective nonlinear parameter ε_e of a micro-inhomogeneous fluid with inclusions. Previously, using Formulas (12)–(16), it was possible to calculate the derivative $\partial\mathcal{K}/\partial P'$, which, in the case of non-resonant bubbles ($\mathcal{K} \approx {\beta'}_S$), is equal to

$$\partial\mathcal{K}/\partial P' = \partial\beta'/\partial P' \approx -\gamma/{P'}^2 = -{\beta'}_S/P', \tag{23}$$

where ${\beta'}_S$ is the adiabatic compressibility of gas in bubbles ${\beta'}_S = \gamma/P$. In the general case of a liquid with bubbles, the expression for the nonlinear parameter takes the form:

$$\varepsilon_e = \varepsilon\left\{1 + \frac{\varepsilon'{\beta'_S}^2}{\varepsilon\beta_S{}^2}\hat{X}\left[1 - \frac{1}{\varepsilon'{\beta'_S}^2}\frac{\partial\beta'}{\partial P'}\left(1 - \frac{\partial\mathcal{K}}{\partial P'}/\frac{\partial\beta'}{\partial P'}\right) + \frac{2}{\varepsilon'}\frac{\mathcal{K}}{\beta'_S}\left(1 - \frac{\mathcal{K}}{\beta'_S}\right)\right]\right\}\left[1 + \hat{X}\frac{\mathcal{K}}{\beta_S}\right]^{-2}, \quad (24)$$

where $\varepsilon' = (\gamma' + 1)/2$. In the case of non-resonant bubbles, the following expression can be obtained:

$$\varepsilon_e \approx \varepsilon\frac{1 + x\left(\varepsilon'{\beta'_S}^2/\varepsilon\beta_S{}^2\right)}{\left[1 + x(\beta'_S/\beta_S)\right]^2}, \quad (25)$$

which has a maximum at $x_m = 2\left(\varepsilon\beta_S{}^2/\varepsilon'{\beta'_S}^2\right)$ and is approximately equal to $(\varepsilon_e/\varepsilon)_m \approx (3/4)(\varepsilon'\beta'_S/\varepsilon\beta_S)^2$.

By making further simplifications and leaving only the resonant characteristics and the main contribution to the scattering amplitude associated with the monopole component of the inclusions vibrations, it is possible to calculate a parameter ε_e that will depend on the structure of the medium, as well as on the dynamic properties of the inclusions. In the case of gas bubbles, the value ε_e is defined as:

$$\varepsilon_e \approx \varepsilon\left(1 + \hat{X}\frac{\mathcal{K}^2\varepsilon'}{\beta_S{}^2\varepsilon}\right)\left[1 + \frac{\mathcal{K}}{\beta_S}\right]^{-2}. \quad (26)$$

The contribution to the sound absorption coefficient α_b caused by bubbles can be presented in the following form, taking into account Formula (20) [18,26]:

$$\alpha_b \approx \frac{\omega}{c}\mathrm{Im}\sqrt{1 + \hat{X}\frac{\mathcal{K}}{\beta_S}} \approx \frac{\omega}{c}\mathrm{Im}\left[1 + \frac{4\pi}{3}\frac{\rho c^2}{\gamma P_0}\int_0^\infty \frac{g(R)dR}{q(R,\omega)}\right]^{1/2}. \quad (27)$$

As can be seen from Formulas (26) and (27), to determine the acoustic characteristics of a liquid with bubbles, the form of the function $g(R)$ in the widest possible range of variation of R is important. The data on the sound scattering at various frequencies, including full-scale measurements in the near-surface layer of the sea saturated with bubbles, revealed the structure of the bubble size distribution function $g(R)$, which, according to [18,26], can be represented by the formula:

$$g(R,z) = A_g R^{-n(z)}\exp\left[-m\left(\frac{R_p}{R} + \frac{R}{R_m}\right)\right]e^{-z/L}, \quad (28)$$

where for the sea conditions $L \approx (2-4)\cdot 10^{-3}U_{10}{}^{2.5}$ (here, L is given in meters, and wind speed U_{10} at an altitude of 10 m is given in m/s), the indicator m depends on the state of the sea; m changes from 1 up to 3, but for moderate and calm waves $m \approx 1$. According to Formula (28), the function $g(R,z)$ has a maximum, which is located at $R_p > 10$ microns, while the value R_p depends on the depth. At the same time, for $R > R_p$ there is a power dependence of the bubble size distribution function with an exponential decline with depth. Thus, Formula (28) takes into account the decline of the function $g(R)$ at small R, the presence of a maximum at $R = R_p$, and the limitation of the spectrum from above by the maximum bubble size R_m. The advantage of such a record $g(R)$ is the practicality and speed of the calculations of various parameters of the medium [18]. It is also important that the exponent $n \sim 3.3$ and the critical dimensions R_m and R_P are natural parameters that follow from the Garrett–Lee–Farmer theory (GLF) [27]. The measurements of $g(R)$ on a large factual material under similar conditions of moderate sea conditions give values n in the interval $n \approx 3.3 \div 3.8$ [9–13,18,26–29], which is close enough to the estimate $n \sim 3.3$ obtained for the inertial interval between the sizes R_m and R_P, which follow from the theory of GLF [27].

2.3. Cavitation Strength and Nonlinear Acoustic Parameter of the Liquid, General Relations

The relationship between the cavitation strength ΔP_k and the nonlinear acoustic parameter ε of the liquid was discussed in [30], in which a dependence of the following form was obtained:

$$\Delta P_k = \frac{1}{2\sqrt{3}} \frac{1}{(\varepsilon - 1)\beta} \tag{29}$$

where $\Delta P_k = P_0 - P_k$; P_0 is the hydrostatic pressure in the liquid; P_k is the threshold pressure of cavitation in the liquid; and β is the compressibility of the liquid. For a pure liquid, the expression ΔP_k essentially represents the intramolecular pressure from the van der Waals equation of state and, by taking into account the mechanism of thermal heterophase fluctuations, can be written as [17–20]:

$$\Delta P_{k0} = \left(16\pi\sigma^3/3kT\ln(C/J)\right)^{1/2}, \tag{30}$$

where σ is the surface tension coefficient, k is the Boltzmann constant, J is the intensity of nucleation, i.e., the number of growing embryos of a new phase per unit volume per unit time, which usually takes the value $J \sim 1$ cm^{-3}s^{-1}, then $\ln(C/J) \approx 70$–78. For water, $\Delta P_{k0} \approx 140$ MPa, and from (30), it follows that $\varepsilon \approx 5$, which is consistent with the values for pure water.

Equation (29) is also generalized to the case of a micro-inhomogeneous liquid containing phase inclusions. Then, in Equation (29), the parameters ε and β should be replaced everywhere by ε_e and β_e—effectively the nonlinear parameter and compressibility of the liquid with inclusions, as determined by Equations (11) and (24)–(26). Taking into account these dependencies, we can write the following formula for cavitation strength:

$$\Delta P_k = \Delta P_{k0}\left[1 + x\frac{\beta'}{\beta\delta}\right] / \left[1 + x\frac{\gamma'\beta'^2}{\varepsilon\beta^2\delta^2}\right], \tag{31}$$

where x is the volume concentration of bubbles and δ is the attenuation constant of resonant bubbles at the frequency ω. It follows from (31) that when $x > x_* = \varepsilon\beta^2\delta^2/\gamma'\beta'^2 \approx 10^{-10}$, we have:

$$\Delta P_k = \Delta P_{k0}(x_*/x). \tag{32}$$

At high concentrations of bubbles, $x > x_{**} = \beta\delta/\beta' \approx 10^{-5}$, the cavitation strength tends to a minimum value:

$$\Delta P_{k,min} = \Delta P_{k0}\frac{\varepsilon\beta\delta}{(2\varepsilon' - 1)\beta'} = \Delta P_{k0}\frac{\varepsilon}{(2\varepsilon' - 1)}x_{**} \approx 10^{-5}\Delta P_{k0}, \tag{33}$$

from which we obtain $\Delta P_{k,min} \approx 10^4$ Pa.

Figure 1 shows a typical dependence $P_k(x)$ in a wide range of values for water at 20 °C at different frequencies of the acoustic field causing cavitation. The hydrostatic pressure is 0.1 MPa. It can be seen that with an increase in frequency, the cavitation strength increases, and with an increase in the concentration of bubbles, it first decreases sharply and then, when the concentration exceeds the value of 10^{-4}, stabilization occurs—it strives for a constant value of cavitation strength, regardless of the concentration of bubbles.

Let us consider the concentration dependence $P_k(x)$ at different pressures as a model for studying the behavior of the cavitation threshold at different depths in the sea. Figure 2 shows a typical dependence of low-frequency cavitation strength $P_k(x)$ in a wide range of values x at various hydrostatic pressures. It can be seen that with an increase in hydrostatic pressure, the cavitation strength increases.

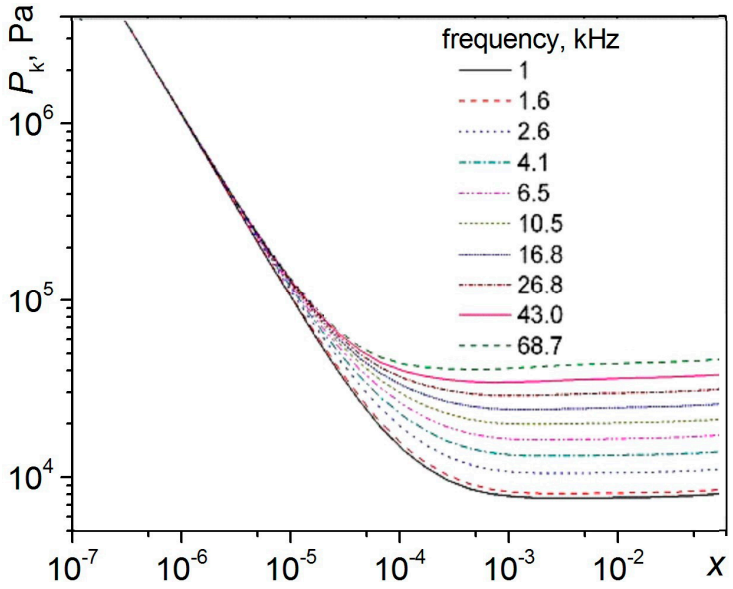

Figure 1. Dependence $P_k(x)$ for water at 20 °C at different frequencies of the acoustic field.

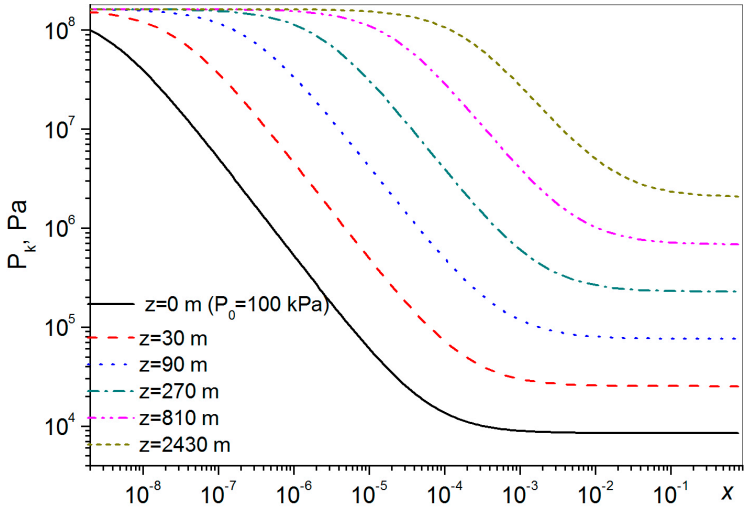

Figure 2. Dependence $P_k(x)$ at different hydrostatic pressures.

2.4. Rectified Gas Diffusion and Bubble Growth Thresholds—Gas Cavitation Threshold

In the previous section, we talked about the threshold of the so-called vapor cavitation in a liquid, in which the threshold is determined by the creation of a critical nuclei and its further growth in the liquid without taking into account the diffusion of gas into the bubble under the influence of sound. Often, in practice, the liquid contains gas bubbles that have formed in the liquid due to the presence of dissolved gas in it. The threshold for the formation of a critical nuclei and its further growth under these conditions depends on the concentration of the dissolved gas relative to the equilibrium concentration of dissolution in the liquid of this gas [16,18,19].

To calculate the threshold, it is necessary to calculate the compressibility of the bubble $\mathcal{K}$, taking into account the effects of gas diffusion. In the expression for the compressibility of inclusion $\mathcal{K}$, the terms related to relaxation due to the processes of gas diffusion exchange in the dynamics of bubbles should be added, when periodically alternating processes of gas exchange occur through the surface of the bubble with gas dissolved in the liquid. In this case, the refined expressions for compressibility $\mathcal{K}$ should be added to Equations (12)–(16). To do this, we use small values of the typical equilibrium concentration of dissolved gas

in a liquid $c_\sigma \approx 10^{-5}$–10^{-6}. In addition, attention should be paid to the smallness of the diffusion coefficient $D_c \approx 10^{-9}$ m^2/s; finally, we obtain:

$$\mathcal{K}_c = \frac{K_c(R,\omega)}{q(R,\omega)},\ K_c(R,\omega) = K(R,\omega)\left[1 - 3c_\sigma \frac{1 - ik_\sigma R}{(k_\sigma R)^2}\right], \tag{34}$$

where $k_\sigma = (i\omega/D_c)^{1/2}$. It can be seen from (34) that the additional term begins to play a significant role only at radii smaller by about an order of magnitude of the diffusion wavelength in a liquid, i.e., at $R < 0.1\lambda_\sigma = (2D_c/\omega)^{1/2}$. Thus, it turns out that at high frequencies, the contribution of diffusion to the intrinsic compressibility of the gas bubble can be neglected. However, at low frequencies with a slow gas diffusion process for small bubbles, it can play a significant role, as can be seen from Formula (34).

Solving the equations of the dynamics of a vapor–gas cavity in a liquid with dissolved gas averaged over the period of the sound field, it is possible to obtain expressions for the average values of the physical quantities in a liquid and in a bubble [18]. The crosslinking of the obtained values at the boundary makes it possible to determine the change in the time averages of the values set on the surface of the vapor–gas bubble. Note that these changes are quadratic in the amplitude of the sound field.

$$P_k = \left\{\left[\Delta c_0 + 3c_\sigma\left(\frac{\partial c_\sigma}{\partial T}\right)_\sigma \Delta T_0\right] / \left[B_q(R,\omega) + B_v(R,\omega)\right]\right\}^{1/2}, \tag{35}$$

where in the form $\Delta c_0 = c_0 - c_\sigma$ and $\Delta T_0 = T_\sigma - T_0$ are indicated by supersaturation with gas and overheating of the liquid on the surface of the bubble. The mechanisms of rectified mass transfer, which are quadratic in the amplitude of the sound field, are contained in the sum $B_q(R,\omega) + B_v(R,\omega)$ and discussed in a number of papers [4,17–19].

Figures 3 and 4 show the growth thresholds $P_k(R,\omega)$ depending on the radii of the bubbles and the frequency of the sound field in water at different water temperatures (at different gas concentrations in the bubbles), as calculated by Formula (35) based on the theory presented in [18]. It follows from Figure 3 that near the Minnaert resonance and the second maximum of the function $\mathcal{K}_c(R,\omega)$, the dependence $P_k(R,\omega)$ takes minimal values. It should be noted that the threshold $P_k(R,\omega)$ in this area may be significantly lower than the known Blake threshold [4,16], as determined by the approximate formula $P_k = 2\sigma/R$ and represented in Figure 3b by a dashed purple line. The growth threshold $P_k(R,\omega)$ depends in a complex way on the parameters of the medium and the frequency of the external field.

Figure 4 shows the dependences of the bubble growth thresholds at different concentrations of gas c_0 dissolved in the liquid, respectively; these concentrations are below the equilibrium concentration for a given temperature and external pressure in the liquid and equal to the equilibrium concentration c_σ. Figure 4 shows that the threshold for the growth of the vapor–gas bubbles decreases sharply with an increase in the concentration of gas dissolved in the water. Thus, the mechanism of the rectified diffusion of gas simultaneously with the mechanism of rectified heat transfer turns out to be essential for vapor–gas bubbles, and therefore, the concentration of gas dissolved in a liquid should always be taken into account when comparing theoretical and experimental results.

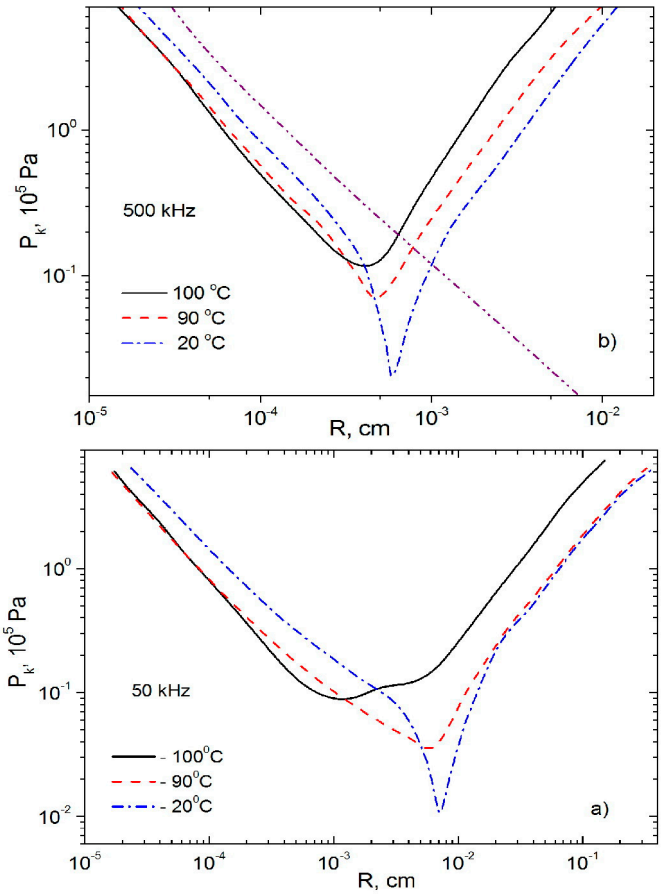

Figure 3. Thresholds for the growth of vapor–gas bubbles in water at frequencies of 50 kHz—(**a**) and 500 kHz—(**b**); the concentration of dissolved gas in water is below equilibrium concentration at different temperatures $c_0/c_\sigma = 0.8$.

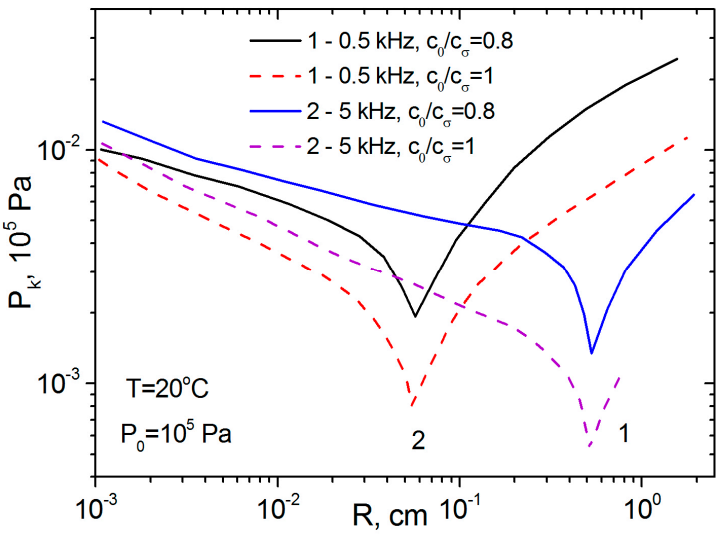

Figure 4. Thresholds for the growth of vapor–gas bubbles in water at frequencies of 0.5 kHz and 5 kHz at different concentrations of dissolved gas in water (solid lines—$c_0/c_\sigma = 0.8$, dashed lines—$c_0/c_\sigma = 1$).

2.5. Experimental Methods and Equipment

The measurements of the nonlinear parameter, according to the method described above and according to Equation (9), were carried out for the first time in the V.I. Il'ichev Pacific Oceanological Institute Far Eastern Branch of the Russian Academy of Sciences (POI FEB RAS) on 12 and 16 expedition cruises of the RV "Academician Alexander Vinogradov" (1988, 1990) in the frequency range from 4 to 40 kHz at various depths [18]. The experimental setup for measuring the nonlinear parameter in various waters of the voyage included an outboard part with receiving and transmitting acoustic antennas and a measuring electronic part, which were connected to each other by connecting cables. The outboard part was a square platform with a side length of 1 m made of 30 cm thick foam, to which an acoustic parametric antenna was attached using a thin halyard. The length of the antenna suspension could vary. The radiation in the working position occurred upwards, towards the surface. The receiving antenna recorded the signal reflected from the water surface. A raft with an antenna could be released from the side of the vessel on an exhaust halyard at a distance of up to 150 m. The sending signal and the echo signals from the receiving antenna were transmitted via separate cables to the electronic measuring part on board the vessel.

Subsequently, to study the distribution of nonlinearity at great depths, a nonlinear acoustic probe was created; the main elements of the probe were a parametric emitter and a cell of a certain length, inside which a biharmonic sound pulse propagated [25], emitted by a parametric emitter. To study the fine structure of the near-surface layer of seawater, the probe made measurements in a small layer of water limited by the cell length, while in the process of lowering (or lifting), a layer-by-layer measurement of a nonlinear parameter, the volume scattering coefficient, and sound attenuation occurred. Thus, the researcher obtained a fine structure of water with a high spatial resolution.

The essence of the measurements in the probe is that the emitted biharmonic pulse propagates in a space bounded on the one hand by a reflecting plate and on the other hand by the emitter itself. The pulse is repeatedly reflected from the plate and the emitter, which makes a large run in a small volume of space, while the accumulation of nonlinear effects occurs, particularly in the growth of a non-linearly generated wave of difference frequency. The selective amplifier of the receiving path allocates the difference frequency, digitizes it, and transmits it to the processing processor. The attenuation coefficient is measured by the decay of the amplitude of the repeatedly reflected pulses of the pumping frequency.

Figure 5 shows the functional diagram of the probe and the frequency spectrum on the receiving hydrophone when the parametric emitter emits a biharmonic signal of 698 kHz and 716 kHz. The submerged probe itself is a 70 cm long rod, at one end of which a parametric emitter is fixed; the radiation axis of the emitter is directed along the axis of the rod towards the reflecting plate fixed at the opposite end. A parametric piezoceramic emitter with a resonant frequency of 650 kHz has a diameter of 66 mm and a directivity characteristic width of 2 degrees. A digital programmable arbitrary waveform generator GSPF-053 was used in the radiation path, the signals of which were amplified by a U7-5 power amplifier and additionally by a radiation unit with a built-in signal switch that allows the receiving of a pulse reflected from the plate in pauses between parcels. The operating frequency range of the pump is in the range of 650–750 kHz. The reception path of the nonlinearity meter is based on the selective amplifier SN-233, which allows the qualitative separation of the acoustic signals of the difference frequency of the nonlinearity meter from the pumping signals and has a gain of up to 10^6. Data entry into the computer was carried out using a 12-bit multichannel ADC board L783, manufactured by L-Card with a maximum quantization frequency of 3 MHz. Other ADCs were also used in the experiments. Their parameters are shown in Table 1. Table 1 presents the main parameters of the typical experimental equipment used for conducting the experiments.

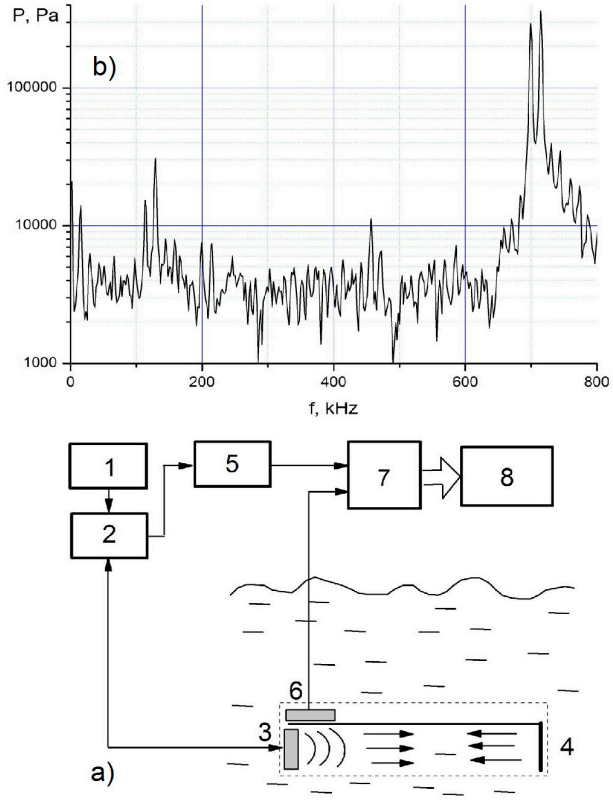

Figure 5. Functional diagram of the probe for measuring the nonlinear acoustic parameter of water (**a**) and the frequency spectrum on the receiving hydrophone (**b**) when emitting a biharmonic signal of 698 kHz and 716 kHz: 1—path of generation and emission of parametric pulses; 2—switch of radiation-reception signals; 3—parametric emitter; 4—reflecting plate; 5—selective difference frequency signal amplifier; 6—depth sensor; 7—two-channel ADC; 8—computer.

Table 1. Main parameters of experimental equipment.

Type	Main Characteristics
Acoustic emitters	650 kHz emitter: directivity 2°, power 1 kW.
Equipment for the emission of acoustic signals	1. Digital signal generator GSPF-053 (Rudnev and Shilyaev, Moscow, Russia): 12 digits, frequency up to 10 MHz, voltage 5 V. 2. Broadband power amplifier U7-5(Etalonpribor, Moscow, Russia): frequency up to 3 MHz, power 20 W, voltage 20 V. https://www.etalonpribor.ru/catalog (accessed on 10 April 2022). 3. BIP power amplifier (V.I. Il'ichev Pacific Oceanological Institute, Vladivostok, Russia): frequency up to 1 MHz, power 600 W, voltage up to 400 V.
Equipment for receiving acoustic signals	1. Selective nanovoltmeter SN-233(Pribor-59, Perm, Russia): standard frequency up to 150 kHz, extended frequency up to 200 kHz; selectivity: (a) wide band, (b) 20 dB/octave, (c) 36 dB/octave, (d) 54 dB/octave; maximum gain 10^6. (https://pribor-59.ru/selectivnye-voltmetry accessed on 18 May 2021). 2. Third-octave filters RFT01018 (Robotron, German Democratic Republic (East Germany)): frequency up to 200 kHz, switchable selectivity: (a) octave, (b) 1/3 octave; maximum gain 10. 3. Brüel & Kjær, Copenhagen, Denmark type 2650 amplifier: frequency up to 200 kHz, LF and HF filters: 30 kHz and 2 kHz, maximum gain 10^2 4. Microphone amplifier RFT00011 (Robotron, German Democratic Republic (East Germany)): frequency up to 1 MHz, maximum gain 10^6
Equipment for recording acoustic signals	1. La2 USB ADC (Rudnev and Shilyaev, Moscow, Russia): quantization frequency up to 400 kHz, 14 digits, 16 channels, maximum gain 10^3. https://rudshel.ru/show.php?dev=35 (accessed on 20 October 2023) 2. ADC E20-10 (L-Card, Moscow, Russia): quantization frequency up to 10 MHz, 14 digits, 4 channels, maximum gain 10^2. https://www.lcard.ru/products/external/e20-10 (accessed on 20 October 2023) 3. ADC board L783. (L-Card, Moscow, Russia): quantization frequency up to 2.8 MHz, 12 digits, 32 channels, maximum gain 10^2. https://www.lcard.ru/products/boards/l-783 (accessed on 20 October 2023)

2.6. Measurement Results of a Nonlinear Parameter

2.6.1. Measurements of a Nonlinear Parameter in the Near-Surface Layer of the Ocean

Figure 6 shows the results of the measurements of the nonlinear acoustic parameter of the near-surface layer of the waters of the North Pacific at various frequencies (averaged data) obtained on a number of expeditions of the RV "Academician A. Vinogradov" in 1988 and 1990 [18]. The frequency dependences of the nonlinear parameter of seawater, approximating the experimental values by the least squares method, can be written as the power dependence $\varepsilon_e = A_\varepsilon F^n$. The frequency dependence $\varepsilon_e(F)$ is due to the presence of bubbles in the near-surface layer of the sea, the nonlinear oscillations of which cause the dependence on the frequency of the nonlinear parameter. As a rule, with a decrease in the difference frequency F, the value of the nonlinear parameter $\varepsilon_e(F)$ increases. At the same time, the values ε_e can reach the values $\varepsilon_e > 100$, which are 20–30 times higher than the values ε for pure (without inclusions) seawater.

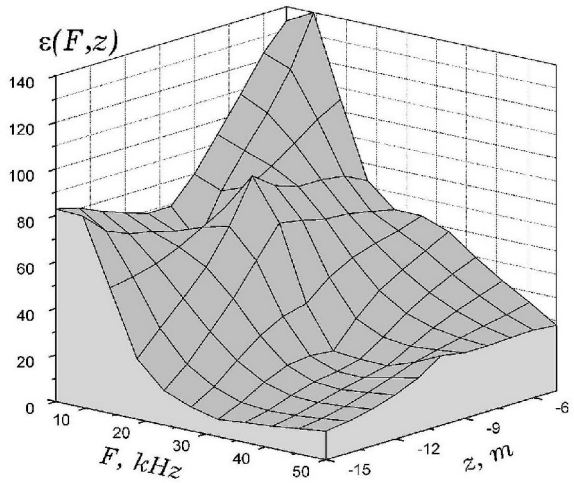

Figure 6. Nonlinear parameter of the subsurface layer of the subarctic waters of the North Pacific (averaged data).

The function $\varepsilon_e(F)$ depends on the concentration of bubbles in the near-surface layer, the value of which in turn varies depending on the depth. At the same time, the value of the nonlinear parameter also changes. Figure 6 shows a near-surface layer with a characteristic thickness of h~5–10 m, depending on the frequency. Summarizing the results discussed above, we can propose the following empirical dependences of the nonlinear parameter on frequency and on depth:

$$\varepsilon_e(F, z) = A_\varepsilon F^n \exp(-z/h). \quad (36)$$

The obtained values reflect our understanding of the influence of the near-surface layers of bubbles on the magnitude of the nonlinear parameter of seawater.

2.6.2. Measurements of a Nonlinear Parameter in the Upper Ocean Layer

A nonlinear acoustic probe was used in the experiments to study the nonlinearity of seawater in the upper layer of the northern Indian Ocean to the depth of the thermocline location of about 100 m during a circumnavigation expedition on the sailboat "Nadezhda" in 2003 [18].

Figure 7 shows a typical sounding schedule conducted in the center of the Arabian Sea of the Indian Ocean at one of the stations. Curve 3 shows the relative change in the nonlinear acoustic parameter of seawater $\varepsilon_{\exp}(z)$ from depth; curve 1 shows the relative change in temperature with depth. From the value of the nonlinear parameter on the surface of the sea, $\varepsilon_0 = 6.1$, it can be seen that the nonlinear parameter changes significantly with depth. As an estimate of curve 2, the distribution of the calculated parameter $(\varepsilon/\varepsilon_0)_{th}$

is presented; it was obtained on the basis of data from UNESCO [31] for the speed of sound $c(T, P, s)$ as a function of temperature T, pressure P, and salinity s.

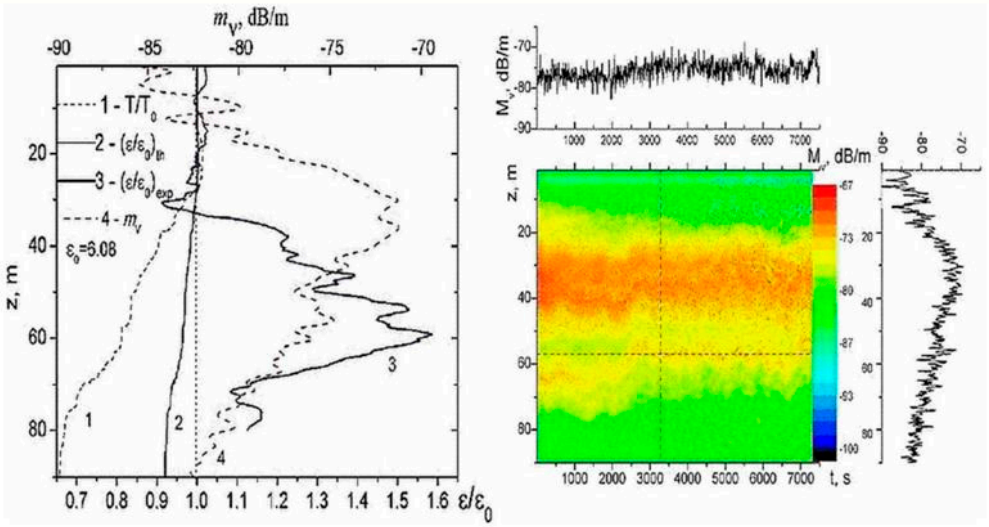

Figure 7. The dependences of the nonlinear parameter $\varepsilon_{\exp}(z)$ on the depth z, significantly exceeding the calculated dependences $\varepsilon_{th}(z)$ for pure water and indicating the presence of an additional contribution associated with the presence of micro-inhomogeneities in the sea and recorded using the sound scattering coefficient M_V: 1—temperature $T(z)/T_0(z=0)$; 2—$\varepsilon_{th}(z)$; 3—$\varepsilon_{\exp}(z)$ at a frequency of 15 kHz (pumping 700 kHz); 4—$M_V(z)$ at a frequency of 100 kHz.

From the comparison of the calculated and experimental results for $(\varepsilon/\varepsilon_0)_{th}$ and $(\varepsilon/\varepsilon_0)_{\exp}$ (curves 2 and 3), it can be seen that these results differ significantly, which indicates that the nonlinearity in seawater is mainly due to the presence of the micro-heterogeneities of various origins in it. Curve 4 in Figure 7 on the right shows the measurements of the sound scattering coefficient m_V at a frequency of 100 kHz. A comparison of the obtained results shows that the change in the nonlinearity parameter diverges from the maximum absolute values of the sound scattering coefficients m_V, and a significant change is observed slightly below the maximum horizon m_V; it coincides with the position of the internal wave, which is usually present at the boundaries of the sound scattering layers, in places of large gradients of the sound scattering coefficient.

2.6.3. Measurements of a Nonlinear Parameter on the Shelf of the Sea of Japan

On the sea shelf, the behavior of the characteristics in the near-surface layer is characterized by great variability. Measurements of nonlinearity were carried out using a nonlinear acoustic probe in Vityaz Bay from aboard a boat that was adrift, according to the method described in [25]. The meter was lowered manually from the side; at the same time, the signal of the difference frequency and the depth of immersion were recorded. The signal with frequencies of 698 and 718 kHz was emitted periodically with an interval of 40 ms. The repeatedly reflected signal was recorded by the computer via the ADC board. The nonlinear acoustic parameter was determined using Equation (6).

Figure 8 shows the dependence of the nonlinearity parameter on the depth in the water area of Vityaz Bay (the Sea of Japan) when lowering the meter from the surface to a depth of 21 m, in the absence of sea waves. The results indicate the presence of a pronounced near-surface layer up to 5–10 m thick with increased nonlinearity, which is observed even in relatively calm water without wave collapse and the formation of bubble clouds.

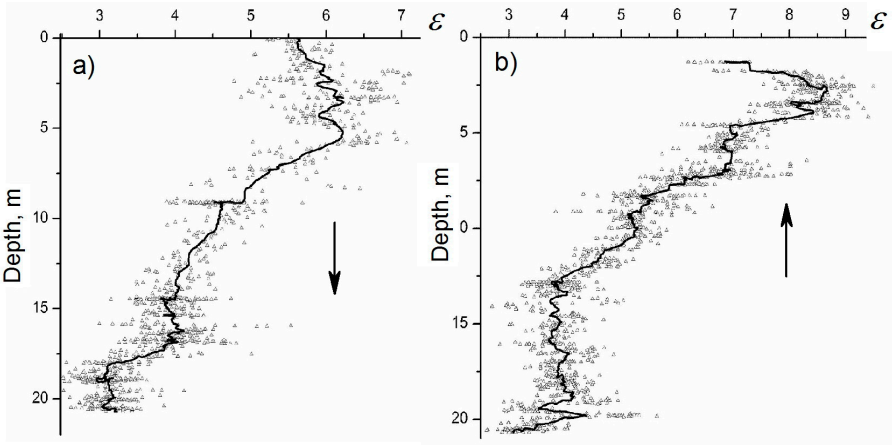

Figure 8. Dependences of the nonlinearity parameter on the depth in the water area of Vityaz Bay (the Sea of Japan) with different soundings: (**a**)—from the surface to a depth of 21 m, (**b**)—from a depth of 21 m upwards.

The most impressive results on the acoustic properties of the near-surface layer of the sea are the results obtained during periods of strong wind over the sea. The effects of the collapse of wind waves produce numerous bubble clouds, which, along with nonlinear properties, are effective absorbers of the energy of the sound waves propagating in the sea. The experimental data on the concentration of bubbles in the near-surface layers of the seawater and Equation (28) allow us to determine additional acoustic nonlinearity, as well as additional sound attenuation introduced by bubbles distributed in the water. Figure 9 shows changes in the bubble concentration over time, the sound absorption coefficient at a frequency of 138 kHz, and the parameter of acoustic nonlinearity of seawater in the near-surface layer of bubbles. It can be seen that the acoustic parameters vary widely with collapses of surface waves and strong wind, leading to modulations of the acoustic properties in the near-surface layer of the sea.

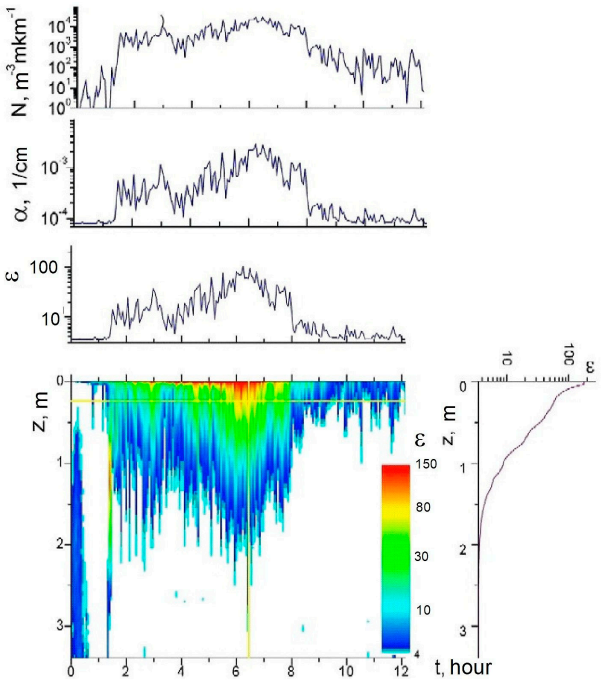

Figure 9. The time change in the near-surface layer of the sea with a sharp change in wind strength and the manifestation of the relationship of acoustic nonlinearity ε, sound absorption α, and bubble distribution in the near-surface layer of the sea (in $m^{-3}mkm^{-1}$) at a depth of z, marked by a horizontal line in the lower figure.

2.7. Acoustic Cavitation Criteria and Cavitation Strength of Seawater

The experimental studies of the cavitation strength of seawater were carried out using an acoustic radiator in the form of a hollow cylinder with a resonant frequency of 10 kHz. Cavitation was recorded by acoustic noises inherent in the cavitation regime [5,18]. The noises were recorded using measuring hydrophones of the company "Akhtuba" (operating frequency band 0.01–300,000 Hz) and the company Bruel & Kjaer, type 8103 (operating frequency band 0.01–200,000 Hz). The signals were recorded digitally using a multichannel 14-bit E20-10 card from L-Card with a maximum digitization frequency of 5 MHz. High voltage was applied to the emitter at a resonance frequency of 10.7 kHz using a Phonic XP 5000 type power amplifier with a maximum power of 2 kW and adjustable inductance compensating for the capacitive load at the resonance frequency. When probing in marine conditions, the hydrophone was attached from the outside of the concentrator near the free end. The relationship between the acoustic characteristics measured by the hydrophone outside and inside the radiator was previously established. Appropriate amendments were subsequently made to the readings of the external hydrophone during the experiments in marine conditions.

When conducting the cavitation studies, special attention was focused on studying the dependence of the cavitation threshold on various criteria for detecting a discontinuity in seawater: by the nonlinearity of the radiated power curve at the frequency of the radiated signal ω_s; by the second harmonic $P_{2\omega}$; and by the total higher harmonics $\sum\limits_{\omega>\omega_s} P_\omega$, as well as by the subharmonics $P_{\omega/2}$ and $P_{3\omega/2}$ [5,18].

Figure 10 shows the dependences of the various spectral components of acoustic noise on the emitter voltage: the total noise for $\omega > \omega_s \sum\limits_{\omega>\omega_s} P_\omega(U_{source}(t))$ and the subharmonic signal $P_{3\omega/2}(U_{source}(t))$ at a frequency of $(3/2)\omega_s$, as well as higher harmonics noise for $\omega > 5\omega_s \sum\limits_{\omega>5\omega_s} P_\omega(U_{source}(t))$. The depth at which the model of the cavitation strength meter was located was 3 m.

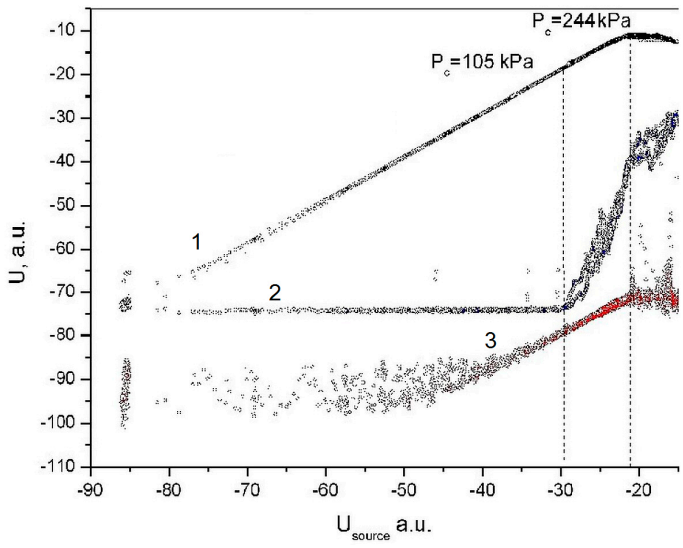

Figure 10. The dependence of the spectral components of acoustic noise on the voltage at the emitter $U_{source}(t)$: 1 is the total noise for $\omega > \omega_s - \sum\limits_{\omega>\omega_s} P_\omega(U_{source}(t))$, 2 is the subharmonic signal $P_{3\omega_s/2}(U_{source}(t))$, 3 is the higher harmonics noise for $\omega > 5\omega_s - \sum\limits_{\omega>5\omega_s} P_\omega(U_{source}(t))$.

It can be seen from Figure 10 that it is possible to clearly distinguish two cavitation thresholds that differ by more than two times: by the curve 3 bend $\sum\limits_{\omega>5\omega_s} P_\omega(U_{source}(t))$ and by the beginning of the asymptotics of all the listed curves and, especially, the curve $\sum\limits_{\omega>\omega_s} P_\omega(U_{source}(t))$. The first threshold of 105 kPa corresponds to the beginning of cavita-

tion, and the second threshold of 244 kPa corresponds to the beginning of violent cavitation, accompanied by a sharp decrease in acoustic impedance. Thus, the criterion of the cavitation threshold is to a certain extent quite conditional. Nevertheless, from the standpoint of the precise detection of the beginning of cavitation, as the beginning of the discontinuity of the continuity of the liquid and the beginning of the formation of bubbles in the liquid, the cavitation strength of the liquid in this example can be considered as the first threshold, which is $P_{c1} = 105$ kPa.

Figure 11 shows the time dependences of various spectral components of acoustic noise: a subharmonic signal $P_{3\omega/2}(t)$ at a frequency of $(3/2)\omega_s$, total harmonics $P_{\Sigma\omega}(t) = \sum_{\omega} P_{\omega}(t)$ in the frequency range from 1 kHz to 1 MHz, and higher harmonics $P_{\Sigma 6\omega}(t) = \sum_{\omega > 5\omega_s} P_{\omega}(t)$, starting from the 6th harmonic 64.2 kHz. The depth at which the model of the cavitation strength meter was located was 3 m. It can be seen that the first threshold of $P_{c1} = 105$ kPa corresponds to the beginning of cavitation, and the second threshold of $P_{c2} = 244$ kPa, located in the asymptotic section $P_{\Sigma\omega}(t)$, corresponds to the beginning of violent cavitation.

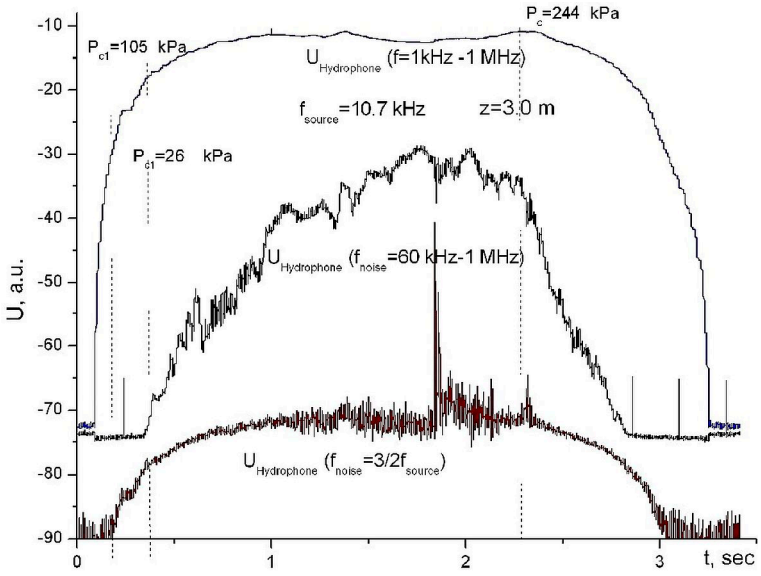

Figure 11. Dependences on the time of the subharmonic signal $P_{3\omega/2}(t)$, total harmonics $P_{\Sigma\omega}(t)$ in the frequency range from 1 kHz to 1 MHz, and higher harmonics $P_{\Sigma 6\omega}(t)$, starting from the 6th harmonic.

The experimental studies of the cavitation strength of seawater were carried out in the autumn period in the Vityaz Bay of the Peter the Great Gulf of the Sea of Japan. Figure 12 shows the temperature and salinity distributions of seawater depending on the depth. It can be seen that there is a clearly defined upper mixed layer with quasi-homogeneous temperature and salinity, extending to a depth of about 6–8 m. Below is a pronounced jump layer characterized by the high vertical gradients of the hydrophysical parameters of seawater.

Figure 13 shows the cavitation strength of seawater as a function of depth, measured in a series of experiments in the same place in Vityaz Bay, the hydrology of which corresponds to Figure 12. The voltage continuously changed during probing. So, the measurements of each point of cavitation strength were carried out in a certain depth range of about 0.5 m. The individual points in Figure 13 correspond to the specified depth intervals. The data on the first cavitation threshold P_{c1} were taken as a cavitation criterion. The measurement errors of the cavitation strength are indicated on the graph and partly reflect the statistical nature of acoustic cavitation.

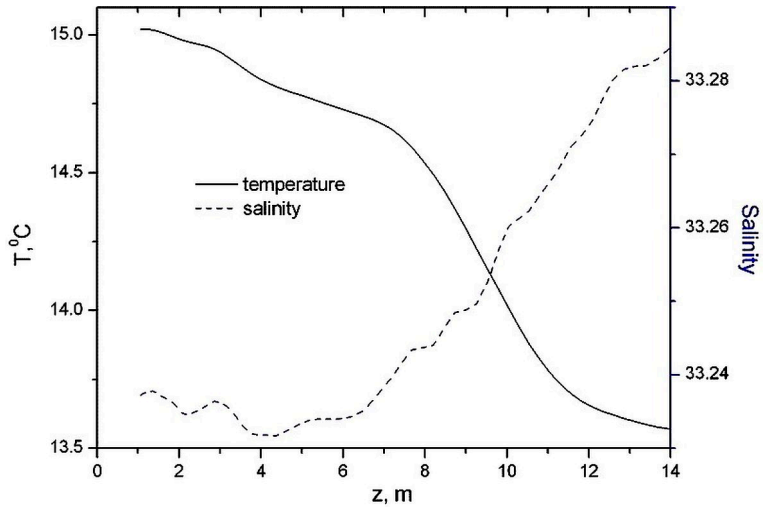

Figure 12. Distribution of temperature and salinity of seawater depending on depth.

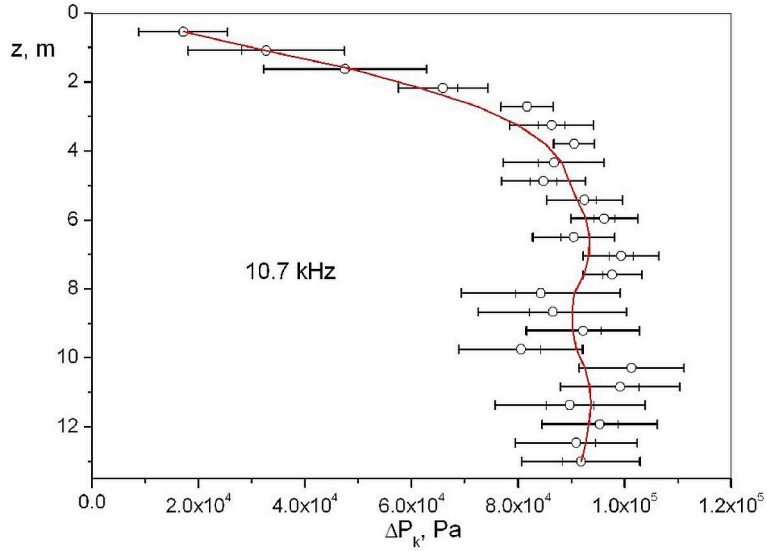

Figure 13. The cavitation strength of seawater depending on the depth: the points at different depths show the measurement results with measurement errors, the standard deviation of which is marked with the error bars; the solid line is the average cavitation strength in the depth.

Figure 13 shows that the cavitation strength of seawater significantly depends on the depth in the subsurface layer up to 6 m thick; then, the dependence on depth is weakly expressed. We associate the obtained results on the decrease in the cavitation strength of seawater in the near-surface layer with the presence of gas bubbles that are always present in this layer. Referring to the theoretical results for the cavitation strength of water with bubbles shown in Figure 1, it can be seen that the experimentally detected decrease to 20 kPa of the cavitation strength of water in the immediate vicinity of the sea surface, which is shown in Figure 13, can be explained by the presence of air bubbles with a total volume concentration of 1.2×10^{-4}.

2.8. Cavitation in Liquid Caused by Optical Breakdown

Experimental complex

The experimental studies of aqueous solutions were carried out on the basis of complexes, including Nd:YAG "Brilliant", "Brio", and "Ultra" lasers, with the following radiation parameters: wavelength 532 nm, pulse duration 10 ns, pulse energy up to 180 mJ, varying in the modulated Q-factor mode, and pulse repetition rate of 1–15 Hz [21–24,32–34].

A typical scheme of the experimental setup is shown in Figure 14. The laser provided a pulsed mode of plasma generation on the surface of the aqueous solutions. The power density of the laser radiation was further increased due to the sharp focusing of the radiation in the desired location (in the liquid, on the surface, or near the surface of the liquid), using lenses with different focal lengths: F = 40 mm, 75 mm, and 125 mm. The optical breakdown was recorded using an optical multichannel spectrum analyzer, the Flame Vision PRO System, with a time resolution of 3 ns, i.e., an optical breakdown occurred in the focusing area, the radiation of which was directed by means of a quartz lens or a light guide to the entrance slit of the Spectra Pro spectrograph coupled with a strobed CCD camera. This scheme provided a delay in the recording of the pulse relative to the beginning of the optical breakdown and varied the exposure time of the signal from 10 ns to 50 microseconds from the beginning of the laser breakdown. Taking into account the variation in delays and exposures, the necessary optimal conditions for recording optical breakdown inside the liquid were found.

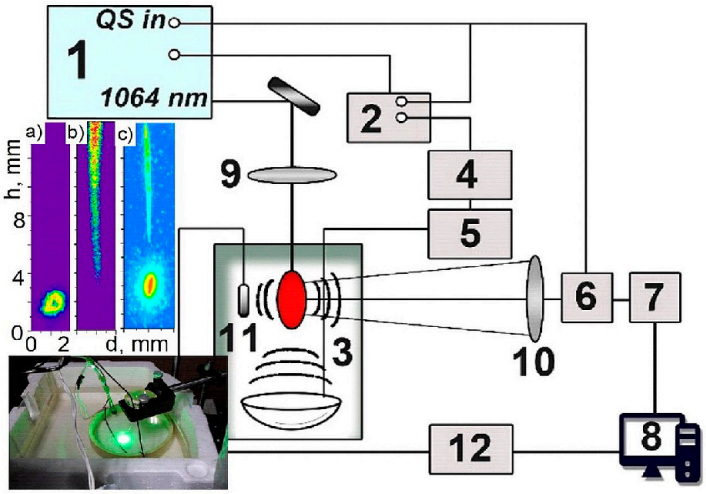

Figure 14. The scheme of the experiment: 1—laser, 2—control pulse switch, 3—piezoceramic ultrasonic emitter (the photo of the emitter is shown on the left), 4—pulse generator of arbitrary shape GSPF 053, 5—power amplifier type U7-5 or Pioneer GM-A3702, 6—delay generator, 7—CCD camera, 8—E20-10 ADC board, 9, 10—rotary mirror and lens, 11—Brüel & Kjær hydrophone type 8103, 12—computer, red oval near hydrophone—breakdown area. Images of laser breakdown of liquid for various types (**a**–**c**) are shown on the left.

Methods of conducting experiments

The optical part of the experiments is traditional, and they were carried out according to the following scheme [32,33]. Laser radiation (1) was focused into a liquid using a rotary mirror and a lens (9). The plasma radiation of the optical breakdown was projected by a lens (10) onto the input slit of a monochromator (7) coupled to a CCD camera. The control was carried out by a computer (8). Various types of breakdown in water were achieved by focusing laser radiation using various lenses. The breakdown occurred either in the depth of the water or in the near-surface layers or in a combination of these two types. Depending on the types of breakdown, different resolutions of the spectral lines were realized.

To analyze the breakdown dynamics and study the parameters of the acoustic wave initiated by optical breakdown, a Brüel & Kjær type 8103 hydrophone was used as a broadband acoustic receiver, the calibration of which at high frequencies was expanded to 800 kHz. Acoustic information was digitized and recorded using a multichannel I/O board from L-Card with a maximum digitization frequency of ~5 MHz. To control ultrasound, an arbitrary pulse generator GSPF 053, a power amplifier, and a resonant cylindrical radiator [34–36] were used, inside which a liquid breakdown occurred in a converging ultrasound field.

2.9. Acoustic Emission Caused by Exposure to Laser Radiation

Experimental data on the spectral density of acoustic emission were obtained under various modes of breakdown in water: for surface breakdown, for breakdown in the water column, and for mixed breakdown. Different modes of breakdown in water were implemented with the different focusing of laser radiation by lenses. As a result, the breakdown occurred either in the water column or in the near-surface layers of the water, or a mixed breakdown was observed, which is a combination of the above types of breakdown. As a result, it turns out that the acoustic emission and the values of the spectral densities of sound differ significantly depending on the nature of the optical breakdown, which can be seen from Figure 15.

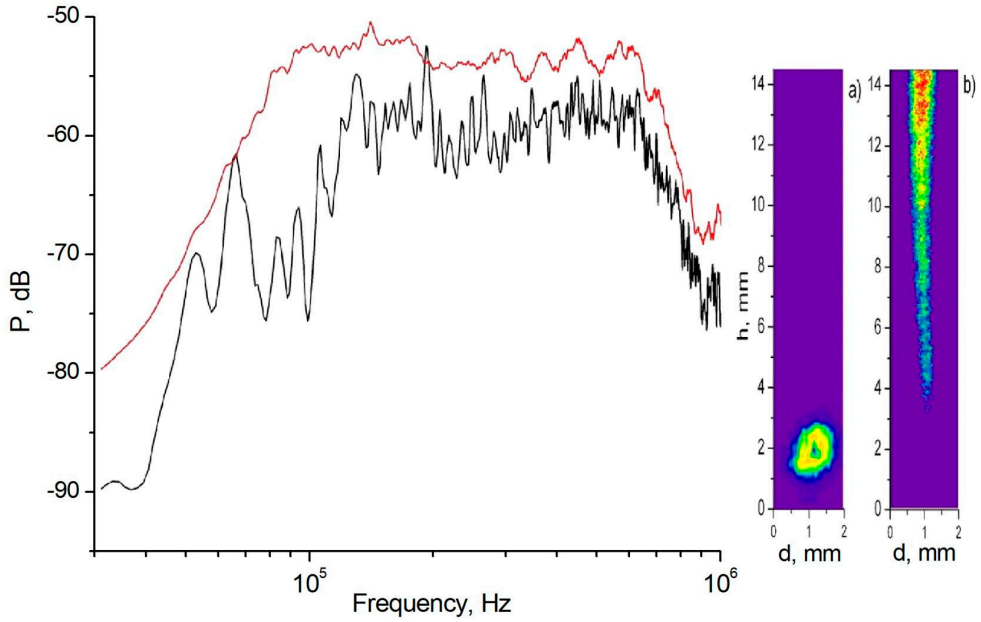

Figure 15. The spectrum of acoustic emission in various separate forms of laser breakdown of water: on the surface (**b**)—black line and in the water column (**a**)—red line.

Simultaneously with the optical breakdown of a liquid in a liquid, a disturbed density region is formed in the vicinity of the breakdown zone, which leads to the formation of an acoustic pulse. Figure 16 shows a recording of a typical acoustic pulse accompanying a liquid breakdown. The distance from the breakdown area to the hydrophone was about 10 cm. Figure 16 shows that a relatively low-frequency component reaches the hydrophone.

The measurement of acoustic emission was used to study the dependence of the efficiency of sound generation on the energy of a laser pulse and its focusing in a liquid.

Figure 17 shows the spectral characteristics of an acoustic wave generated in a liquid by an optical breakdown depending on the energy of the laser pulse. It can be seen from Figure 17 that shifts of the low-frequency maximum to the region of lower frequencies are observed with an increase in the pulse energy. The high-frequency spectral maximum, which is not displaced at all laser pulse energies, is probably related to the natural resonance of the hydrophone at a frequency of ~300 kHz.

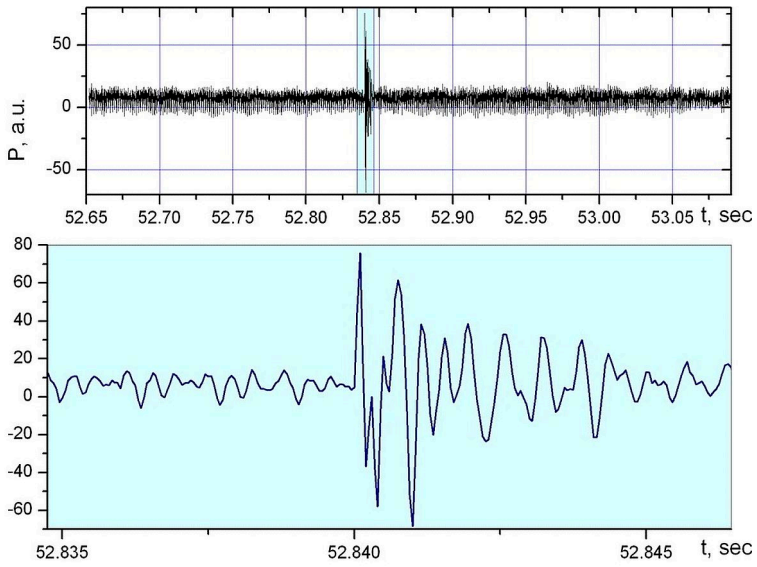

Figure 16. The shape of the acoustic pulse from the breakdown zone received by the hydrophone in the liquid.

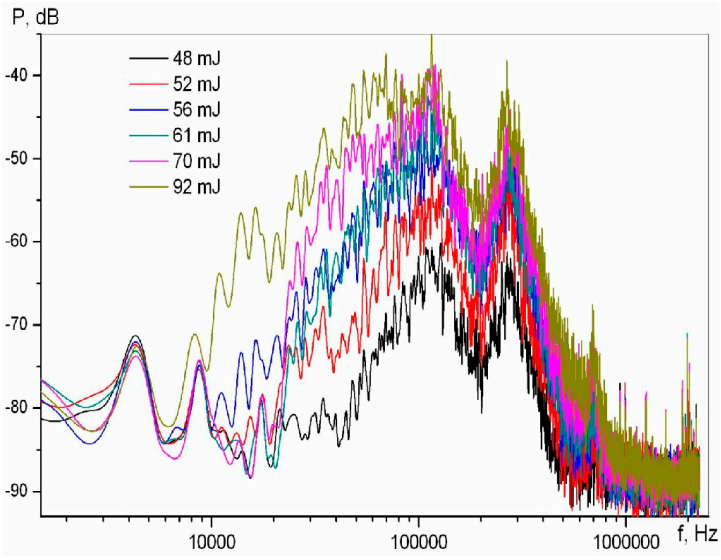

Figure 17. Features of acoustic emission with an increase in the energy of the laser pulse E.

Figure 18 shows the dependence of the sound pressure P on the leading edge of the acoustic pulse on the energy E. Let us analyze the dependence of acoustic emission on the dynamics of bubbles. The method of analysis is as follows. The total energy of the acoustic pulse E_{ac} is calculated as:

$$E_{ac} = \int\limits_{V_{imp}} \langle P(r,t)v(r,t)\rangle dV, \tag{37}$$

where $v(r,t) = -\int_{-\infty}^{t} \nabla_r P(r,\xi)d\xi$, the angle brackets for the function $f(t)$ mean averaging over the duration of the pulse τ of the type $\langle f(t)\rangle = (1/\tau)\int_t^{t+\tau} f(x)dx$. At distances r greater than the radius of the bubble R, $r >> R$, where acoustic emission is registered, the wave front in the registration area can be considered flat, from which we have a relationship between the pressure and the velocity of particles in the wave in the form [3]

$v(r,t) \approx P(r,t)/\rho c$, where ρ is the density and c is the speed of sound in the medium. As a result, we have the total energy of the acoustic pulse E_{ac} in the form

$$E_{ac} = \frac{2\pi r^2}{\rho c} \int_0^\tau P^2(r,t)dt. \tag{38}$$

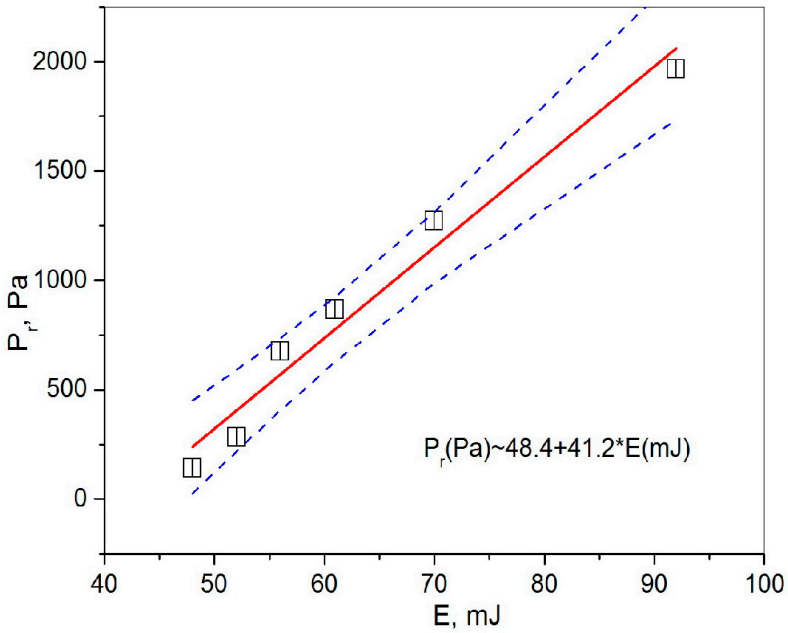

Figure 18. The dependence of the sound pressure P on the leading edge of the acoustic pulse on the energy E: experimental points, linear approximation by the formula indicated on the graph (solid line) and 96% confidence interval of approximation (dashed lines).

Along with the obtained estimates of the total energy of the emitted acoustic pulse, it is of interest to try to solve the inverse problem—to restore the dynamics of the bubble according to the acoustic emission data. The theoretical basis is a formula for the distribution of pressure in the radiated wave from a spherical bubble as a source of monopole radiation, which can be written in the form [3]

$$P_r(t) = \rho\left(R\ddot{R} + 2\dot{R}^2\right)(R/r), \tag{39}$$

where $\dot{R} = dR/dt = U(t)$. By solving a nonlinear differential equation with respect to the function $R(t)$, while considering the function $P(t)$ known on the basis of the experimental data in the received acoustic pulse, it is possible to calculate the function $R(t)$, the velocity of the bubble wall $U(t)$, and the intensity in the acoustic wave:

$$I = \left\langle P_R(t)\dot{R}(t)\right\rangle,\ P_R(t) = (r/R)P_r(t) \tag{40}$$

Figure 19 shows these dependencies, which show that the acoustic data can reproduce the function $R(t)$, which is consistent with the characteristic dependencies $R(t)$ obtained from the direct measurements of optical breakdown images at the late stages of their evolution.

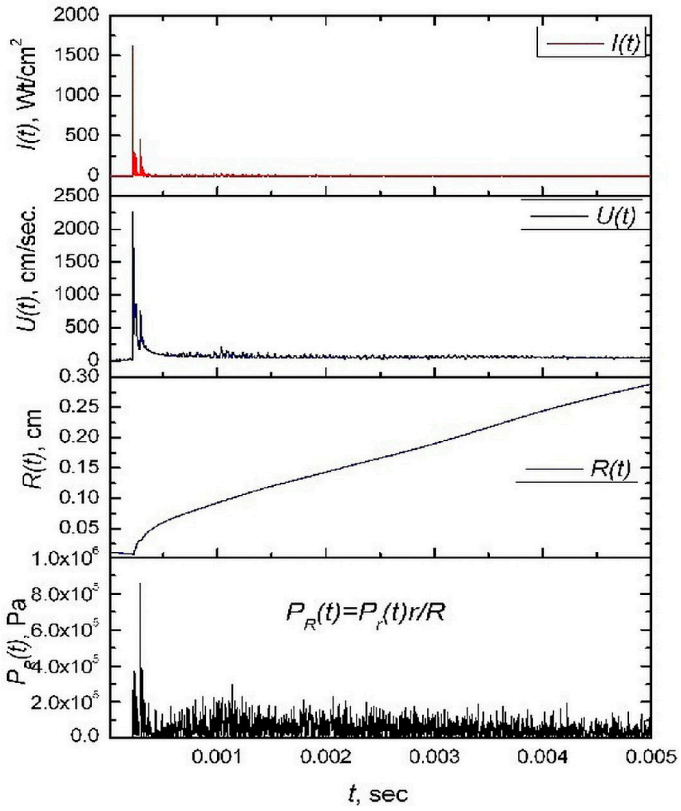

Figure 19. Acoustic emission and bubble dynamics (from **bottom** to **top**): time dependence of pressure $P(t)$ in the received acoustic pulse on the optical breakdown region; function $R(t)$ calculated by Formula (35) from data for $P(t)$; function $dR(t)/dt$, constructed for calculated function $R(t)$; intensity in the emitted acoustic pulse $I(t)$.

3. Discussion of the Results

The main attention in the article was focused on the description of the experimental methods and theoretical foundations that allow the obtaining and analyzing of the experimental data on the effective parameters of micro-inhomogeneous liquids. Real liquids always contain phase inclusions, among which bubbles are the most significant with regard to the changing of the properties of liquids. Theoretical estimates of the effective parameters of such bubble liquids are carried out in the article. All the calculations were carried out in the framework of a homogeneous approximation, while the calculations of the bubble dynamics were used in the framework of a linear approximation to analyze the complex effective compressibility of a micro-inhomogeneous liquid. The resonance and relaxation (thermal and diffusion) characteristics of the bubbles, as well as their size distribution, were taken into account.

Previously conducted studies of the distribution of bubbles in typical real liquids (including seawater) allowed this article to use the model function of bubble size distribution (28) to calculate the effective compressibility β_e (11) and, on this basis, to obtain estimates for the absorption coefficient α and the speed of sound c_e, Equations (21) and (22), which were valid for sufficiently high concentrations of bubbles. The article did not have the opportunity to discuss the limits of applicability of the approximations made, but the authors, when conducting the analysis, understood the need to take into account the effects of multiple scattering and the overlap of sound scattering cross-sections at high concentrations of bubbles; therefore, all the calculations were carried out in areas where these effects should not be significant.

The effective nonlinear parameter of a micro-inhomogeneous liquid was estimated under the assumption that the main contribution is made by the nonlinearity of radially symmetric bubble pulsations, the contribution of which differs for bubbles with different

sizes. In this regard, it was important to take into account the dimensional effects near the monopole resonance and the relaxation near the "second resonance"—the maximum compressibility when the bubble size coincides with the heat wavelength, which led to the general Formula (26). The estimates of the nonlinearity parameter obtained on this basis and measured experimentally by the methods analyzed in Section 2.1 showed the similarity of the results obtained, which is illustrated by the graphs in Figures 6–9. Here, attention should be paid to the practicality of using the nonlinear acoustic probe described in the article when using a parametric emitter in marine research. The probe allows you to obtain a fine structure of water with high spatial resolution.

The calculation of the tensile strength of a liquid is usually carried out by taking into account the theory of thermal heterophase fluctuations and the analysis of the size composition of the nuclei. In the article, we took as a basis Equation (29) obtained in [30] for a pure liquid. However, it was not difficult to also generalize Equation (29) to a micro-inhomogeneous liquid. As a result, it was possible to link various characteristics of a micro-inhomogeneous liquid with simple formulas. Such a phenomenological approach allowed us to obtain Equation (31) for cavitation strength ΔP_k, which at low concentrations gives the tensile strength of a pure liquid and at high concentrations of bubbles $x > x_{**} = \beta\delta/\beta' \approx 10^{-5}$ gives the minimum values of $\Delta P_{k,min} \approx 10^{-5}\Delta P_{k0} \approx 10^4$ Pa. As the concept of cavitation is a rather multilateral phenomenon, which is characterized by various approaches to measuring cavitation strength, this article, in Section 2.4, gives a small overview of the theoretical estimates of the alternative approaches to the cavitation threshold based on the effects of rectified heat transfer and rectified gas diffusion, which in conditions of gas saturation of a liquid can lead to a sharp decrease in cavitation thresholds, which is illustrated in Figures 3 and 4. Later, in Section 2.7, the dependence of the various criteria of the cavitation threshold for detecting a discontinuity in seawater was studied: by the nonlinearity of the radiated power curve at the frequency of the radiated signal; by the second harmonic; and by the total higher harmonics, as well as by the subharmonics. Two cavitation thresholds were identified, of which the first threshold corresponds to the beginning of cavitation, and the second to the beginning of violent cavitation, accompanied by a sharp decrease in acoustic impedance. In the work, from the standpoint of the precise detection of the beginning of cavitation, as the beginning of the discontinuity of the continuity of the liquid and the beginning of the formation of bubbles in the liquid, a threshold was chosen, which can be conditionally considered the cavitation strength of the liquid. Figure 13 shows that for the selected cavitation threshold, the cavitation strength of seawater significantly depends on the depth in the subsurface layer up to 6 m thick; then, the dependence on depth is weakly expressed, which indicates a connection with the presence of gas bubbles, which are always present in the subsurface layer; this is shown clearly in Figure 9.

Unfortunately, it was not possible to measure cavitation strength by acoustic methods below a depth of 14 m due to significant experimental difficulties in creating cavitation at the ultrasound frequencies used. In connection with this circumstance, the optical breakdown in the liquid was studied, and the connection with the cavitation strength was established. The obtained dependences of the sound pressure P at the leading edge and the spectral characteristics of the generated acoustic pulse on the energy E of the laser pulse causing the optical breakdown allowed us to estimate the dynamics of the breakdown region based on acoustic emission data.

By comparing the data obtained for the cavitation strength of water presented in Figures 13 and 19, one can see the fairly close values of the experimental measurements of the cavitation strength obtained by the acoustic method and by using laser breakdown. The lower graph of Figure 19 shows an estimate of the pressure $P_R(t)$ on the wall of the cavity at which a breakdown occurs, which turned out to be close to the value of the cavitation strength in seawater at a depth of 5 m.

Here, we assume that such a coincidence is not accidental, i.e., the cavitation strength of liquids in the case of vapor cavitation, when there are no gas bubbles, will correspond

to the boiling temperature threshold of the liquid when it is locally overheated by a laser pulse, provided that the corresponding overheating ΔT_k is associated with the cavitation strength by dependence $\Delta T_k = (dT/dP)_\sigma \Delta P_k$, where $(dT/dP)_\sigma$ corresponds to the slope of the phase equilibrium curve of the liquid–vapor.

This assumption needs to be thoroughly verified, especially at the high hydrostatic pressures corresponding to the great depths of seawater, for which, according to Figure 2, there is a strong dependence of cavitation strength on depth. The use of an independent assessment of the cavitation threshold of a liquid using a laser breakdown of a liquid may be of practical importance if it is necessary to measure cavitation strength at great depths in marine conditions where it is extremely difficult to realize high acoustic pressure values using traditional radiators. The use of optical cavitation would be a way out of this situation due to the use of a completely different mechanism of discontinuity of the medium—induced laser pulse boiling, which corresponds in all parameters to the formation of a critical nuclei of a new phase and its further growth in the supercritical region to macroscopic dimensions. It is this mechanism that is usually implemented during cavitation in the absence of gas bubbles, which significantly facilitate the rupture of the liquid.

4. Conclusions

In the work, within the framework of the homogeneous approximation of a micro-inhomogeneous liquid, the studies of the effective parameter of acoustic nonlinearity and the cavitation strength of a liquid with bubbles were carried out. The analysis used data on the bubble size distribution function in seawater, which were written in the form of a formula that simplified the calculation of the effective parameters of a micro-inhomogeneous liquid.

The relationship of the acoustic nonlinearity parameter, cavitation strength, absorption coefficient, and velocity dispersion with the bubble size distribution function was established, and the typical values of these parameters were calculated for different gas contents in water in the form of bubbles.

Experimental measurements of the acoustic nonlinearity parameter and the cavitation strength of seawater at various depths have been carried out, which are consistent with theoretical estimates. The interrelation of these characteristics for seawater is shown.

Due to the difficulties of measuring cavitation strength by acoustic methods, other methods are being sought. It is proposed to use an optoacoustic method associated with the use of laser radiation, which causes the optical breakdown of optical cavitation, accompanied by a strong sound generation effect. The connection between optical breakdown thresholds and acoustic cavitation thresholds has been established and can later be used to identify cavitation thresholds at high static pressures (at great depths in the sea), where the use of acoustic emitters is extremely difficult.

Author Contributions: Conceptualization, A.V.B. and V.A.B.; methodology, A.V.B., V.A.B. and I.V.K.; software, A.V.B. and E.V.S.; validation, A.V.B., V.A.B. and I.V.K.; formal analysis, A.V.B. and V.A.B.; investigation, A.V.B., V.A.B. and I.V.K.; resources, V.A.B. and A.V.B.; data curation, A.V.B., V.A.B. and E.V.S.; writing—original draft preparation, A.V.B., V.A.B. and E.V.S.; writing—review and editing, A.V.B. and V.A.B.; visualization, A.V.B., V.A.B. and E.V.S.; supervision, A.V.B. and V.A.B.; project administration, A.V.B.; funding acquisition, V.A.B. All authors have read and agreed to the published version of the manuscript.

Funding: The work was carried out within the framework of the state projects: 0211-2021-0002 (reg. No. AAAAA-A20-120031890011-8), 0211-2021-0007 (reg. No. 1210215000054-3) and FFMM-2024-0032.

Data Availability Statement: Data are contained within the article.

Conflicts of Interest: The authors declare no conflict of interest.

References

1. Hovem, J.M. *Marine Acoustics: The Physics of Sound in Underwater Environments*; Peninsula Publishing: Newport Beach, CA, USA, 2012; 656p.
2. Beyer, R.T. The parameter B/A. In *Nonlinear Acoustics*; Hamilton, M.F., Blackstock, D.T., Eds.; Academic Press: Cambridge, MA, USA, 1997; pp. 25–39.
3. Naugolnykh, K.A.; Ostrovsky, L.A. *Nonlinear Wave Processes in Acoustics*; University Press: Cambridge, UK, 1998; 298p.
4. Leighton, T.G. *The Acoustic Bubblel*; Academic Press: San Diego, CA, USA, 1994.
5. Akulichev, V.A.; Il'ichev, V.I. Thresholds of acoustic cavitation in sea water in various areas of the World ocean. *Phys. Acoust.* **2005**, *51*, 167–179. [CrossRef]
6. Brekhovskikh, L.M.; Lysanov, Y.P. *Fundamentals of Ocean Acoustics*; Springer: Berlin, Germany, 2013; 250p.
7. Karpov, S.; Prosperetti, A.; Ostrovsky, L. Nonlinear wave interactions in bubble layers. *J. Acoust. Soc. Am.* **2003**, *113*, 1304–1316. [CrossRef]
8. Holliday, D.V.; Greenlaw, C.F.; Thistle, D.E.; Rines, J.E.B. A biological source of bubbles in sandy marine sediments. *J. Acoust. Soc. Am.* **2003**, *114*, 2317–2326. [CrossRef]
9. Baschek, B.; Farmer, D.M. Gas Bubbles as Oceanographic Tracers. *J. Atmos. Ocean. Technol.* **2010**, *27*, 241–245. [CrossRef]
10. Vagle, S.; McNeil, C.; Steiner, N. Upper ocean bubble measurements from the NE Pacific and estimates of their role in air-sea gas transfer of the weakly soluble gases nitrogen and oxygen. *J. Geophys. Res.* **2010**, *115*, C12054. [CrossRef]
11. Czerski, H. An inversion of acoustical attenuation measurements to deduce bubble populations. *J. Atmos. Ocean. Technol.* **2012**, *29*, 1139–1148. [CrossRef]
12. Liu, R.; Li, Z. The effects of bubble scattering on sound propagation in shallow water. *J. Mar. Sci. Eng.* **2021**, *9*, 1441. [CrossRef]
13. Czerski, H.; Brooks, I.M.; Gunn, S.; Pascal, R.; Matei, A. Ocean bubbles under high wind conditions—Part 1: Bubble distribution and development. *Ocean Sci.* **2022**, *18*, 565–586. [CrossRef]
14. Novikov, B.K.; Rudenko, O.V.; Timoshenko, V.I. *Nonlinear Underwater Acoustics*; American Institute of Physics: New York, NY, USA, 1987.
15. Grelowska, G.; Kozaczka, E. Nonlinear properties of the Gotland deep—Baltic Sea. *Arch. Acoust.* **2015**, *40*, 595–600. [CrossRef]
16. Neppiras, E.A. Acoustic cavitation. *Phys. Rep.* **1980**, *61*, 159–251. [CrossRef]
17. Caupin, F.; Herbert, E. Cavitation in water: A review. *Comptes Rendus Phys.* **2006**, *7*, 1000–1017. [CrossRef]
18. Akulichev, V.A.; Bulanov, V.A. *Acoustic Study of Small-Scale Heterogeneities in the Marine Environment*; POI FEB RAS: Vladivostok, Russia, 2017; 414p. Available online: https://www.poi.dvo.ru/node/470 (accessed on 19 December 2023).
19. Lauterborn, W.; Kurz, T. Physics of bubble oscillations. *Rep. Prog. Phys.* **2010**, *73*, 106501. [CrossRef]
20. Padilla-Martinez, J.P.; Berrospe-Rodriguez, C.; Aguilar, G.; Ramirez-San-Juan, J.C.; Ramos-Garcia, R. Optic cavitation with CW lasers: A review. *Phys. Fluids* **2014**, *26*, 122007. [CrossRef]
21. Cremers, D.A.; Radziemski, L.J. *Handbook of Laser–Induced Breakdown Spectroscopy*; John Wiley& Sons: New York, NY, USA, 2006; 282p.
22. Musazzi, S.; Perini, U. *Laser-Induced Breakdown Spectroscopy*; Springer Series in Optical Sciences 182; Springer: Berlin/Heidelberg, Germany, 2014; 575p.
23. Kudryashov, S.I.; Lyon, K.; Allen, S.D. Photoacoustic study of relaxation dynamics in multibubbles systems in laser–superheated water. *Phys. Rev. E* **2006**, *73*, 055301. [CrossRef]
24. Byun, K.T.; Kwak, H.Y.; Karng, S.W. Bubble evolution and radiation mechanism for laser–induced collapsing bubble in water. *Jpn. J. Appl. Phys.* **2004**, *43*, 6364–6370. [CrossRef]
25. Bulanov, V.A.; Korskov, I.V.; Popov, P.N. Measurements of the nonlinear acoustic parameter of sea water via a device using reflected pulses. *Instrum. Exp. Technol.* **2017**, *60*, 414–417. [CrossRef]
26. Farmer, D.M.; Vagle, S.; Booth, D. Reverberation effects in acoustical resonators used for bubble measurements. *J. Acoust. Soc. Am.* **2005**, *118*, 2954–2960. [CrossRef]
27. Garrett, C.; Li, M.; Farmer, D. The Connection between bubble size spectra and energy dissipation rates in the upper ocean. *J. Phys. Oceanogr.* **2000**, *30*, 2163–2171. [CrossRef]
28. Bulanov, V.A.; Bugaeva, L.K.; Storozhenko, A.V. On sound scattering and acoustic properties of the upper layer of the sea with bubble clouds. *J. Mar. Sci. Eng.* **2022**, *10*, 872. [CrossRef]
29. Deane, G.B.; Preisig, J.C.; Lavery, A.C. The suspension of large bubbles near the seasurface by turbulence and their role in absorbing forward-scattered sound. *IEEE J. Ocean. Eng.* **2013**, *38*, 632–641. [CrossRef]
30. Sehgal, C.M. Non-linear ultrasonics to determine molecular properties of pure liquids. *Ultrasonics* **1995**, *33*, 155–161. [CrossRef]
31. Fofonoff, N.P.; Millard, R.C., Jr. Algorithm for computation of fundamental properties of seawater. In *UNESCO Technical Papers in Marine Science*; No. 44; UNESCO: Paris, France, 1983.
32. Bukin, O.A.; Salyuk, P.A.; Maior, A.Y.; Golik, S.S.; Il'in, A.A.; Bulanov, A.V.; Baulo, E.N.; Akmaikin, D.A. The use of laser spectroscopy methods in the Investigation of the carbon cycle in the ocean. *Atmos. Ocean. Opt.* **2010**, *23*, 328–333. [CrossRef]
33. Ilyin, A.A.; Nagorny, I.G.; Bukin, O.A.; Bulanov, A.V.; Shmirko, K.A. Features of development of optical breakdown on an inclined aluminum surface. *Tech. Phys. Lett.* **2012**, *38*, 975–978. [CrossRef]
34. Bulanov, A.V.; Nagorny, I.G.; Sosedko, E.V. A study of the optical and acoustic spectral characteristics by laser breakdown of water in an ultrasonic field. *Tech. Phys. Lett.* **2019**, *45*, 1200–1203. [CrossRef]

35. Bulanov, A.V.; Sosedko, E.V. Opto-acoustic effects by laser breakdown of seawater in an ultrasonic field. *Dokl. Earth Sci.* **2020**, *491*, 183–186. [CrossRef]
36. Bulanov, A.V. Using of ultrasound in automated laser induced breakdown spectroscopy complex for operational study of spectral characteristics of seawater of carbon polygons. *Bull. Russ. Acad. Sci. Phys.* **2022**, *86*, S32–S36. [CrossRef]